International Journal of Transportation Science and Technology 11 (2022) 360–380

Contents lists available at ScienceDirect

International Journal of Transportation Science and Technology

journal homepage: www.elsevier.com/locate/ijtst

Freeway tunnel effect of travel time based-on a double lane traffic model

Yongliang Zhang [a], M.N. Smirnova [b,c,d], Jian Ma [a,e], Zuojin Zhu [a,b,*], N.N. Smirnov [b,c,d]

[a] Faculty of Engineering Science, University of Science and Technology of China, Hefei 230026, China
[b] Faculty of Mechanics and Mathematics, Lomonosov Moscow State University, Moscow 119992, Russia
[c] Scientific Research Institute for System Analysis, Russian Academy of Sciences, Moscow, Russia
[d] Moscow Center for Fundamental and Applied Mathematics, Moscow 119991, Russia
[e] Naval Architecture and Civil Engineering, Jiangsu University of Science and Technology, Jiangsu Province 215600, China

A R T I C L E I N F O

Article history:
Received 24 November 2020
Received in revised form 6 February 2021
Accepted 6 May 2021
Available online 21 May 2021

Keywords:
Double lane traffic flow model
Freeway tunnel
Speed limit of freeway tunnel
Travel time
Weighted essentially non-oscillatory scheme

A B S T R A C T

Speed limit of freeway tunnel restricts car driving behaviors. To explore the tunnel effect of travel time, a double lane traffic model is put forward, and a *compensative function* of mean travel time is simply introduced in this paper. The model describes the net lane-changing rate using the ratio of characteristic lane changing time to traffic relaxation time, assumes that the cars on both lanes of the tunnel have the same equilibrium speed, but the speeds on both lanes of normal section are different. It is assumed that the road length is 100 km, and the tunnel length is 7.5 km except for the case of seeking tunnel length effects. The model is used to build a simulation platform. Numerical results indicated that when the initial road density normalized by jam density is above 0.2, the tunnel causes a congestion region just upstream the tunnel inlet, provides a smooth region just downstream the tunnel outlet, can affect the traffic flow pattern significantly. But the tunnel effect of travel time is small, as the tunnel can merely slightly increase the mean travel time. The on/off ramp flows play a crucial role in the formation of traffic flow pattern.

1. Introduction

Since traffic flow has significant influences on the life and work of human beings, many macroscopic traffic flow models have been developed, among which are the well-known model LWR (Lighthill and Whitham, 1955; Richards, 1956), the Euler model (Payne, 1971), the gas-kinetic-based model (Helbing and Treiber, 1998; Hoogendoorn and Bovy, 2000), the Navier–Stokes like model (Kerner and Konhäuser, 1993), the conserved anisotropic model (Zhang et al., 2009), and the generic model (Lebacque and Mammar, 2013; Lebacque and Khoshyaran, 2013), even though the model developers have to face the criticism of Daganzo (1995).

A literature review for the development of macroscopic traffic flow model and the background for travel time prediction were given in the work about urgent-gentle class traffic flow model (Zhang et al., 2018a). To estimate freeway traffic time, a generic approach was proposed by Li and Souleyrette (2016). More recently, an analytical model, named vehicular malicious information propagation (VMIP), has been proposed (Wang et al., 2019). The model is designated for platooned traffic (one-

* Corresponding author.
E-mail address: zuojin@ustc.edu.cn (Z. Zhu).

https://doi.org/10.1016/j.ijtst.2021.05.002
2046-0430/

Nomenclature

A	Jacobian matrix
B_k	a parameter defined by Eq. (8)
B_{*k}	a parameter used to in traffic pressure definition (10)
B_{0k}	a parameter used to in traffic pressure definition (10)
c	traffic sound speed, (m/s)
c_0	sound speed at second critical density, (m/s)
$c_{\tau k}$	traffic saturation speed defined by Eq. (9),
G	modulus of vehicular fluid elasticity, $(\text{veh} \cdot \text{m/s}^2)$
K_k	a parameter used to in traffic pressure definition (10)
l	average vehicle length, (m)
l_0	length scale, (m)
p	traffic pressure, $(\text{veh} \cdot \text{m/s}^2)$
R/ρ	traffic flow acceleration
X_{t1}	position of tunnel inlet (km)
X_{t2}	position of tunnel exit (km)
X_{brj}	braking distance on lane j for $j = 1, 2$, in the tunnel for $j = 3$ (m)
X_{Rk}	kth ramp intersection
X_I	$I =$ A, B, C, D, E positions of initial traffic jams (km)
v_{f1}	free flow speed on lane I in the normal section, (m/s)
v_{f2}	free flow speed on lane II in the normal section, (m/s)
v_{f3}	speed limit of freeway tunnel, (m/s)
u	traffic speed, (m/s)
u_e	equilibrium speed, (m/s)
v_0	speed scale, (m/s)
L	total length of ring road, (km)
L_t	tunnel length, (m)
α	$= l\rho_m$
$\beta_{\star}$	ratio of lane-changing time to relaxation time
γ	traffic flow elasticity, (m^2)
ρ	traffic density, (veh/km)
ρ_m	traffic jam density, (veh/km)
σ	random parameter to describe ramp flow
$\sigma^{\star}_{av}$	normalized mean travel time defined by Eq. (43)
τ	relaxation time, (s)

Abbreviation

DLM	double lane traffic model
EZM	extended Zhang's model (EZM) (Zhang, 2003)
MFD	macroscopic fundamental diagrams
WENO5	fifth-order weighted essentially non-oscillatory scheme

lane, particularly). It was numerically confirmed that the model can efficiently describe the interactions between traffic dynamics and malicious information spreading; and the information propagation highly depends on traffic flow patterns.

For road condition studies, Zhang et al. (1996) considered the ramp control problem as a dynamic optimal process to minimize the total time spent in a freeway system, which is comprised of a freeway section and its on/off ramps. Under the restriction that the controlled freeway has to serve all of its ramp demand, and the traffic flow adheres the rules prescribed by the LWR theory with a triangular flow-density fundamental diagram, when ramp metering is beneficial to the system in terms of total time savings, or otherwise, some solution techniques to the problem were provided, with some preliminary numerical results and empirical validation.

Considering congested condition downstream from off-ramps often propagate upstream blocking all freeway lanes and affecting traffic that does not cause the bottleneck, Günther et al. (2012) proposed a methodology to determine the flow of competing cars to be detoured to under-utilized roads in the local network in order to improve the systems capacity and reduce total delays under stationary condition.

As sags and tunnels can cause capacity reduction, capacity drop, and extreme low acceleration rates when cars accelerate away from the upstream queue, to explain the three bottleneck effects, Jin (2018) presented a behavioral kinematic wave model which is helpful to develop better design and control strategies to improve the performance of a sag or tunnel bottleneck.

For mutlti-lane traffic, some very general model relating to vehicular flow on a two lane homogeneous road in statistical equilibrium was introduced by Haight (1963), who pointed out only when the assumptions are most stringent is it possible to solve a few problems, and even then the formulas are rather formidable. Macroscopic modelling and analysis were discussed by Michalopoulos et al. (1984), and a gas-kinetic model was proposed by Nagatani (2002). A multi-lane model was proposed (Chang and Zhu, 2006) to analyze the dynamic traffic properties of a freeway segment under a lane-closure operation that often incurs complex interactions between mandatory lane-changing cars and traffic at unblocked lanes. For homogeneous multi-lane freeways, a macroscopic behavior theory of traffic dynamics was proposed (Daganzo, 2002), the theory was described in its fully complexity without calculus, shown to be qualitatively consistent with experimental observations, including puzzling. While recognizing the traffic stream is usually composed of aggressive and timid (or, urgent and gentle) drivers, predictions for separate groups of lanes were made. Building on the continuum macroscopic behavior theory and focusing on the onset of congestion, the behavior of multi-lane freeway traffic past on ramps was further examined (Daganzo, 2002). A two lane model was proposed (Tang et al., 2008), in which the lane-changing model is consistent with car-following behavior on a two-lane freeway; another multi-lane traffic flow model accounting for lane width, lane-changing and the number of lanes was reported late (Tang et al., 2014).

In addition, some investigations relating to microscopic multi-lane traffic modelling can be seen in Davis (2004), Li and Chen (2017) and Liu et al. (2018). A study for the vehicle lane-changing behavior under rainfall conditions using cellular automata was reported by Zhang et al. (2016), they found in the medium and high densities, the rain causes more traffic congestion, and the frequency and duration of traffic congestion in space–time diagram increase accordingly.

A literature review for lane changing was given by Zheng (2014), who reported that there are some modules of lane-changing, such as the multi-lane kinematic wave module (Laval and Daganzo, 2006), and the approach to extend kinematic wave theory (Jin, 2010, 2013).

A numerical approach for the approximation of several widely applied macroscopic traffic flow models was reported (Papageorgiou, 2014), where the family of spatial discretizations includes a second-order monotone upstream-centered scheme for conservation laws (MUSCL) scheme and a fifth-order weighted essentially non-oscillatory scheme (WENO5) improved by Borges et al. (2008).

In this paper, to explore freeway tunnel effect of travel time, a double lane traffic model (DLM) is put forward, and a *compensative function* of mean travel time is simply introduced. Cars on lane I are named urgent (aggressive) as they have a higher free flow speed, with those on lane II named gentle (timid) due to a lower free flow speed. But all cars in freeway tunnel must adhere to the tunnel speed limit. DLM adopts a single instantaneous traffic speed for cars on both lanes, with the net lane change rate expressed by a source term reflecting local traffic inhomogeneity, although from microscopic points of view, overtaking of cars has zero probability if cars on both lanes have the same speed. Such a choice of traffic modeling is in some sense a result of recalling the criticism of Daganzo (1995), as we expect to minimize the number of parameters in the model. DLM uses some parameters such as second critical speed, free flow speed and braking distance to determine the macroscopic fundamental diagrams (MFD) (Kiselev et al., 200). Note that all cars in freeway tunnel must adhere to a same fundamental diagram labeled by tunnel as shown in Fig. 1.

Based on the DLM, a simulation platform is built that can provide grid speed of traffic flow for calculating travel time. Another approach is possibly the simplest from a technological point of view, it uses equilibrium speeds in freeway tunnel and in the normal road segment at uniform initial density to estimate mean travel time through the road, then to improve accuracy of estimation a compensative function is introduced that can be determined by the mean travel time predicted numerically. In the simulation platform, a third-order Runge–Kutta method (Shu, 1988; Shu and Osher, 1989) is adopted to handle time derivative term, a WENO5 scheme (Jiang and Shu, 1996; Henrick et al., 2005) is used to calculate numerical flux.

The paper is organized as below. We will introduce the equations of the DLM in Section 2, describe numerical method in Section 3, report the approaches for travel time in Section 4, discuss the numerical results in Section 5, and finally present the conclusions.

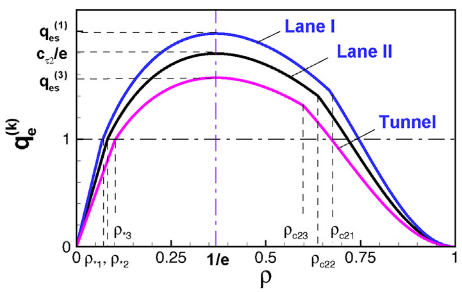

Fig. 1. Fundamental diagram for traffic flows on a double lane road with a freeway tunnel. ρ is measured by jam density ρ_m, the unit of tunnel speed limit v_{f3} is km/h, the flow rate q_e has a unit of $q_0 = \rho_{*2} v_{f2}$, and $q_{es}^{(k)} = c_{\tau k}/e \cdot [\rho_{*k} v_{fk}/q_0]$, k = 1, 2, and 3 respectively for the first lane I, the second lane II, and the tunnel.

2. Equations for a double lane traffic model

Different from the previous multi-lane traffic modelling mentioned in the foregoing section, to avoid mathematical complexity of modelling vehicular flow on a two lane road, the double lane traffic model adopts a single instantaneous traffic speed, and an algebraic expression for traffic pressure. Otherwise, if the model uses two instantaneous traffic speeds, a further parameter has to be adopted to describe the momentum exchange between the two lanes as a result of vehicular lane changing; if the model uses a governing equation for traffic pressure such as in Hoogendoorn and Bovy (2000), the model complexity is largely increased, which does not benefit to the model application.

As shown in Fig. 2, lane I is fast for the running of urgent cars, lane II is slow for the gentle cars. Naturally, the double lane road is similar to the freeway in reality. The phenomenon of lane changing occurs spontaneously to maintain the local homogeneity of car distribution. To describe the double lane traffic flow, the traffic density on lane I and II are labeled by ρ_1 and ρ_2 respectively, lane number averaged traffic density is denoted by $\rho\,[= (\rho_1 + \rho_2)/2]$, with the urgent density fraction given by $s\,[= \rho_1/(2\rho)]$ and lane averaged traffic flow rate represented by $q = \rho u$. As the agency of transportation management naturally stipulates the slow lane in the outer side so that on-ramp cars can get into the road at first on lane II as observed in real freeways, hence the variation rate of ρ_1 should not include any ramp-flow dependent parameter explicitly, lane changing becomes the only reason of source term generation. For the gentle cars on lane II having the attempt of lane changing to become urgent class, in a length of 1 km, its number should be $(\rho - \rho_1)$. If the traffic relaxation time is τ, and the total lane changing time of cars is $(\tau\beta_{\star})$, the net lane-changing rate for lane I should be -$(\rho_1 - \rho)/(\tau\beta_{\star})$. Therefore, using the randomly generated ramp parameter σ as reported (Zhang et al., 2018a), and defining the traffic elasticity by $\gamma = 0.68v\tau$, the DLM equations are

$$\begin{cases} \rho_t + q_x = \sigma q/l_0, \\ \rho(u_t + uu_x) = R, \\ (\rho_1)_t + (\rho_1 u)_x = -(\rho_1 - \rho)/(\tau\beta_{\star}). \end{cases} \tag{1}$$

Note that it is easier for understanding when the source term in the governing equation of ρ_1 is written in the form of $(\rho_2 - \rho_1)/(\tau\beta_{\star})/2$. The reason of taking the present form is traffic density on lane II ρ_2 has not been chosen as a mandatory variable, alternatively, we have selected the lane number averaged density ρ to describe the source term. Where $\beta_{\star}$ is the ratio of characteristic lane changing time to traffic relaxation time (τ), l_0 is the length scale of traffic flow, it is assumed to be the product of sound speed c and traffic relaxation time τ

$$l_0 = c \cdot \tau, \tag{2}$$

according to the classical mechanics, the traffic sound speed is defined by

$$c = \sqrt{\partial p/\partial \rho}. \tag{3}$$

The lane number averaged density ρ is the locally balanced variable at which the lane changing caused source term, i.e., $[-(\rho_1 - \rho)/(\tau\beta_{\star})]$, should vanish. R satisfies the equation (Zhu and Yang, 2013; Ma et al., 2018)

$$R + \left[\rho\gamma(R/\rho)_x\right]_x = (q_e - q)/\tau - p_x + [(2G\tau + \rho v_1)u_x]_x, \tag{4}$$

where traffic elasticity is denoted by γ to distinguish $\sigma, \rho v_1 = 3\rho\gamma u_x, p$ is traffic pressure, q_e is the equilibrium traffic flow obtained by macroscopic fundamental diagram as shown in Fig. 1, R/ρ is traffic flow acceleration, $v = 2G\tau/\rho$ is vehicular fluid kinematic viscosity, with G denoting modulus of vehicular fluid elasticity. The use of Eq. (4) means that we have recognized that the self-organization of traffic flow can be described simply by introducing the viscosity $(2G\tau + \rho v_1)$ and the elasticity γ.

Here to describe ramp flow effects, the dimensionless ramp parameter σ is adopted, which can be estimated by random number generator with Gaussian normal distribution. When local traffic flow q is zero, the source term caused by the ramps should vanish, that is naturally true at off-ramp intersections.

On normal section, urgent and gentle classes cars have different free flow speed and braking distance, the equilibrium speeds of traffic flow for the urgent and gentle classes are also different, as shown in the MFD given by Fig. 1. Let the jam density be ρ_m, the equilibrium speed can be written as

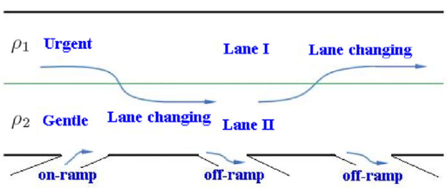

Fig. 2. Illustration of a double lane traffic flow.

$$q_e^{(k)} = \begin{cases} \rho v_{fk}, & \text{for } \rho \leqslant \rho_{*k}; \\ -c_{\tau k}\rho \ln(\rho/\rho_m), & \text{for } \rho_{*k} < \rho \leqslant \rho_{c2k}; \\ B_k \rho\{1 - \text{sech}[\Lambda_k \ln(\rho/\rho_m)]\}, & \text{for } \rho_{c2k} < \rho \leqslant \rho_m. \end{cases} \tag{5}$$

Where the subscript k and superscript (k) is road condition (schematically shown in Fig. 3) dependent: in the normal section, $k = 1$ and 2, represents the corresponding variables of the urgent and gentle cars respectively; in the freeway tunnel, $k = 3$, denotes the relevant variables of all cars that must adherence to the traffic regulation of tunnel speed limit. Therefore, in the normal section, using the average with respect to the urgent density fraction s, q_e can be calculated by

$$q_e = q_{e2} + (q_{e1} - q_{e2})s, \tag{6}$$

but in the tunnel, it has the form

$$q_e = q_{e3}. \tag{7}$$

At the second critical density ρ_{c2}, traffic flow has an equilibrium speed u_{c2}. Defining a speed ratio $\Lambda_k = c_{\tau k}/u_{c2}$, the parameter B_k can be written as

$$B_k = u_{c2}/\{1 - \text{sech}[\Lambda_k \ln(\rho_{c2k}/\rho_m)]\}. \tag{8}$$

$c_{\tau k}$ is the traffic saturation speed at the saturation density ($\rho/\rho_m = 1/e$), it is calculated by

$$c_{\tau k} = v_{fk}/\ln[1 + X_{\text{brk}}/l], \tag{9}$$

where l is the length of vehicle, X_{brk} is the braking distance. In fact, cars in the tunnel have the demand to follow the tunnel speed limit, suggesting that in the tunnel the MFD for the urgent and gentle cars should be the same. Hence, it is natural and practical to assume that in the tunnel the free flow speed v_{f3} is just the same as the tunnel speed limit, and so are the critical densities ρ_{*3}, ρ_{c23}.

According to the previous work (Zhang et al., 2018b), by assuming that on empty road traffic sound speed is exactly equal to the free flow speed, using pressure model parameter obtained by postulating that the sound speed at the second critical point is exactly equal to the saturation speed $c_{\tau k}$, and defining

$$\begin{cases} K_k = \{c_{\tau k}[1 - \alpha\rho_{c2k}/\rho_m]\}^2, \\ c_{*k}^2 = K_k/(1 - \alpha\rho_{*k}/\rho_m)^2, \\ B_{*k} = \left(v_{fk}^2 - c_{*k}^2\right)/\rho_{*k}^4, \\ B_{0k} = c_{*k}^2\rho_{*k} + B_{*k}\rho_{*k}^5/5 - K_k \cdot \{\rho_{*k}/[1 - \alpha(\rho_{*k}/\rho_m)]\}, c_{0k} = c_{\tau k}, \end{cases}$$

then the traffic pressure p_k has the form

$$p_k = \begin{cases} c_{*k}^2\rho + \frac{1}{5}B_{*k} \cdot \left[\rho_{*k}^5 + (\rho - \rho_{*k})^5\right], & \text{for } \rho \leqslant \rho_{*k}; \\ K_k \cdot \{\rho/[1 - \alpha(\rho/\rho_m)]\} + B_{0k}, & \text{Otherwise.} \end{cases} \tag{10}$$

the corresponding sound speed c_k has the form

$$c_k = \begin{cases} \sqrt{c_{*k}^2 + B_{*k}(\rho - \rho_{*k})^4}, & \text{for } \rho \leqslant \rho_{*k}; \\ K_k^{1/2}/[1 - \alpha(\rho/\rho_m)], & \text{Otherwise.} \end{cases} \tag{11}$$

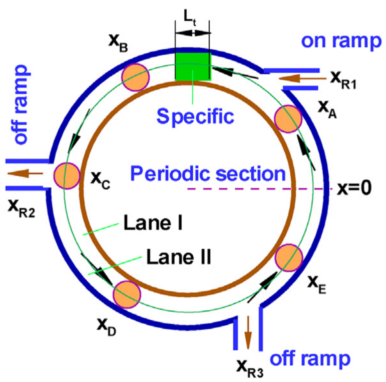

Fig. 3. Schematic diagram of ring traffic flow with a freeway tunnel and five initial jams at $X_I (I = \text{A, B, C, D, E})$. The tunnel inlet is at X_{t1} with the tunnel exit positioned at X_{t2}, hence the tunnel length is $L_t = X_{t2} - X_{t1}$.

The MFD in Fig. 1 labeled by lane I, lane II and tunnel are obtained using the free flow speeds v_{f1}, v_{f2}, v_{f3}, and braking distances $X_{\rm br1}, X_{\rm br2}, X_{\rm br3}$, whose values can be seen in Table 1.

The governing equations of the extended Zhang's model (EZM) (Zhang, 2003) can be written as

$$\begin{cases} \rho_t + q_x = \sigma q / l_0, \\ q_t + \{q^2/\rho\}_x = R, \\ (\rho_1)_t + (\rho_1 u)_x = (\rho - \rho_1)/(\tau\beta_{\star}) \end{cases} \tag{12}$$

with

$$R = (q_e - q)/\tau - p_x - [(2\beta c_0) \cdot (c/c_0)]u_x + [(2\beta c_0) \cdot (c/c_0)\rho]u_{xx},$$

where equilibrium flow $q_e = \rho u_e$ is calculated by Eqs. (5), traffic pressure p and sound speed ratio $c/c_0 = \tau_0/\tau$ are predicted by using the average with respect to s, i.e., the same approach as that used in the DLM. The dimensionless parameter β is given by

$$\beta = \frac{v}{2\tau_0 c_0^2}. \tag{13}$$

The numerical method for Eq. (12) is the same as described in Section 3, but the primary differences from the DLM occurs in the form of q- equation. It is noted that the discretization of $-[(2\beta c_0) \cdot (c/c_0)\rho](q/\rho)_x$ is implemented by a second order upwind scheme (Tao, 2001).

The DLM and ELZ have adopted traffic pressure gradient p_x in describing traffic acceleration R/ρ, indicating that negative speeds in the solutions can possibly occur, as reported by Aw and Rascle (2000). This promotes the development of anisotropic higher-order traffic flow models (Rascle, 2002; Xu et al., 2007; Zheng et al., 2017).

The DLM is characterized by using the same instantaneous speed for both lanes cars to avoid the use of more parameters, and the time ratio $\beta_{\star}$ to describe the net lane changing rate. In comparison with existing lane-changing modules, the module of lane-changing in the DLM is possibly the simplest. The DLM can be used to determine the compensative function of mean travel time estimated by another approach based-on equilibrium speed at uniform initial density. In the DLM reported in Tang et al. (2008), an acceleration equation is derived by analyzing the car-following behavior when lane-changing is allowed. Such equation has not adopted traffic pressure and viscous-elastic term reflecting self-organization of cars; the lane averaged traffic density and flow rate are used, but the ramp effect has not been mentioned. An advantage of the DLM proposed in this paper is the eigenvalues of Jacobian matrix **A** in Eq. (15) can be derived much easier than the multi-class traffic model discussed elsewhere (Zhu et al., 2004; Xie et al., 2006). In particular, the assumption of $c|_{\rho=0} = v_f$ in the DLM should be a favourable strategy for modeling the traffic stoppage problem discussed in Daganzo (1995), as it allows all the elements in the first column of the matrix **A** to be zero, thus makes the traffic flow being described totally not sensitive to the non-uniformity of traffic density.

3. Numerical method

The numerical method for solving the equations of DLM is based on the fifth-order weighted essentially non-oscillatory scheme (WENO5) (Jiang and Shu, 1996; Henrick et al., 2005) and the 3rd order Runge–Kutta scheme (Shu, 1988; Shu and Osher, 1989). The former is adopted to calculate numerical flux, and the latter is used to handle time derivative term.

Using the definition $c^2 = \partial p/\partial \rho, p_x$ can be written as

Table 1
Parameters of traffic flow on ring road.

v_{f1} (km/h)	120	$c_{\tau3}$[1]	4.280	X_B (km)	30
v_{f2} (km/h)	100	ρ_{*1}	0.0676	X_C (km)	50
v_{f3} (km/h)	80	ρ_{*2}	0.0819	X_D (km)	70
$X_{\rm br1}$ (m)	80	ρ_{*3}	0.1021	X_E (km)	90
$X_{\rm br2}$ (m)	65	ρ_{c21}	0.6676	X_{t1} (km)	20
$X_{\rm br3}$ (m)	51	ρ_{c22}	0.6374	L_t[3] (km)	7.5
τ_{01} (s)	6.735	ρ_{c23}[2]	0.5985	ρ_m (veh/km)	172
τ_{02} (s)	9.007	X_{R1} (km)	17	l (m)	5.8
τ_{03} (s)	12.834	X_{R2} (km)	50	l_0(m)	100
Λ_1	2.474	X_{R3} (km)	83	v_0=$\rho_{*2} v_{f2}$ (m/s)	2.2756
Λ_2	2.220	$\sigma_{1\rm av}$	0.1	t_0=l_0/v_0 (s)	43.9445
Λ_3	1.948	$\sigma_{2\rm av}$	[-0.2,0]	L (km)	100
$c_{\tau1}$	5.437	$\sigma_{3\rm av}$	−0.1	$I_{\max} = L/l_0$	1000
$c_{\tau2}$	4.849	X_A (km)	10	$\beta_{\star}$	1

[1] $c_{\tau1}, c_{\tau2}, c_{\tau3}, \Lambda_1, \Lambda_2,$ andΛ_3 are in the unit of v_0;
[2] ρ_{c21}, ρ_{c22}, ρ_{c23}, ρ_{*1}, ρ_{*2}, and ρ_{*3} are measured by ρ_m;
[3] Freeway tunnel length $L_t = X_{t2} - X_{t1}$, and tunnel exit $X_{t2} = X_{t1} + L_t$.

$$p_x = c^2 \rho_x,$$

then by taking $R_1 = R + p_x + \sigma q u / l_0$instead of R, the DLM Eqs. (1) and (4) become

$$\frac{\partial \mathbf{U}}{\partial t} + \frac{\partial \mathbf{F}(\mathbf{U})}{\partial x} = \mathbf{S}, \tag{14}$$

where $\mathbf{U} = (\rho, q, \rho_1)^T, \mathbf{F}(\mathbf{U}) = (q, q^2/\rho + p, \rho_1 \cdot q/\rho)^T$, and $\mathbf{S} = [\sigma q / l_0, R_1, (\rho - \rho_1)/(\tau \beta_{\star})]^T$, with superscript ′$T$′ representing vector transpose.

The eigenvalues of Eq. (14) $a_k, (k = 1, 2, 3)$ may be expressed as $a_1 = u - c$, $a_2 = u + c$, and $a_3 = u$, where the Jacobian matrix is

$$\mathbf{A} = \begin{pmatrix} \frac{\partial F_1}{\partial U_1} & \frac{\partial F_1}{\partial U_2} & \frac{\partial F_1}{\partial U_3} \\ \frac{\partial F_2}{\partial U_1} & \frac{\partial F_2}{\partial U_2} & \frac{\partial F_2}{\partial U_3} \\ \frac{\partial F_3}{\partial U_1} & \frac{\partial F_3}{\partial U_2} & \frac{\partial F_3}{\partial U_3} \end{pmatrix} = \begin{pmatrix} 0 & 1 & 0 \\ -u^2 + c^2 & 2u & 0 \\ -\frac{uU_3}{U_1} & \frac{U_3}{U_1} & u \end{pmatrix}. \tag{15}$$

Label the eigenvalues, the left and right eigenvectors by

$$a_k, \quad \mathbf{l}_k(\mathbf{U}), \quad \mathbf{r}_k(\mathbf{U}), \quad k = 1, 2, 3, \tag{16}$$

then the matrix $\mathbf{A}$ can be written as

$$\mathbf{A} = \mathbf{RaL}, \quad \mathbf{L} = \mathbf{R}^{-1}, \tag{17}$$

where $\mathbf{a} = \mathrm{diag}(a_1, a_2, a_3)$ is a diagonal matrix composed of eigenvalues; $\mathbf{R}$, $\mathbf{L}$ are respectively the left and right characteristic matrix being composed of relevant eigenvectors,

$$\mathbf{R} = [\mathbf{r}_1, \mathbf{r}_2, \mathbf{r}_3], \quad \mathbf{L} = \begin{bmatrix} \mathbf{l}_1 \\ \mathbf{l}_2 \\ \mathbf{l}_3 \end{bmatrix}. \tag{18}$$

Hence, using flux splitting (Shui, 1998), the splitting form of $\mathbf{F}(\mathbf{U})$ can be written as

$$\mathbf{F}^{\pm}(\mathbf{U}) = \mathbf{A}^{\pm}\mathbf{U}, \quad \mathbf{A}^{\pm} = \mathbf{R}\mathbf{a}^{\pm}\mathbf{L}, \tag{19}$$

where

$$\mathbf{a}^{\pm} = \mathrm{diag}(a_1^{\pm}, a_2^{\pm}, a_3^{\pm}),$$
$$a_k^{\pm} = \tfrac{1}{2}(a_k \pm |a_k|), \quad k = 1, 2, 3.$$

The approach of deriving the elements of $\mathbf{R}$ is similar to what described in Ref. (Zhu and Wu, 2003). It is characterized by assuming the k-th element of vector $\mathbf{r}_k$ equals unity, i.e. $r_{kk} = 1$, for $k = 1, 2, 3$. As the Jacobian matrix $\mathbf{A}$ has a special structure with thirteen zero elements, using the assumption $r_{kk} = 1$, one obtains

$$\mathbf{R} = \begin{pmatrix} r_{11} & r_{12} & 0 \\ r_{21} & r_{22} & 0 \\ r_{31} & r_{32} & 1 \end{pmatrix}, \quad \mathbf{L} = \begin{pmatrix} l_{11} & l_{12} & 0 \\ l_{21} & l_{22} & 0 \\ l_{31} & l_{32} & 1 \end{pmatrix}. \tag{20}$$

From Eq. (15), it is seen that $a_{ik} = 0$, for $i = 1, 2$, and $k = 3$, hence we have

$$\mathbf{r}_1 = \begin{pmatrix} r_{11} \\ r_{21} \\ r_{31} \end{pmatrix} = \begin{pmatrix} 1 \\ -\frac{a_{11} - a_1}{a_{12}} \\ -\frac{a_{31} + a_{32} r_{21}}{(a_{33} - a_1)} \end{pmatrix}, \quad \mathbf{r}_2 = \begin{pmatrix} r_{12} \\ r_{22} \\ r_{32} \end{pmatrix} = \begin{pmatrix} -\frac{a_{22} - a_2}{a_{21}} \\ 1 \\ -\frac{a_{32} + a_{31} r_{12}}{(a_{33} - a_2)} \end{pmatrix}. \tag{21}$$

and

$$\left.\begin{array}{l} \begin{pmatrix} l_{11} & l_{12} \\ l_{21} & l_{22} \end{pmatrix} = \frac{1}{1 - r_{12} r_{21}} \begin{bmatrix} 1 & -r_{12} \\ -r_{21} & 1 \end{bmatrix}, \\ (\, l_{31} \quad l_{32} \,) = [\, -(r_{31} l_{11} + r_{32} l_{21}) \quad -(r_{31} l_{12} + r_{32} l_{22}) \,]. \end{array}\right\} \tag{22}$$

These explicit expressions of elements for characteristic matrices $\mathbf{R}$ and $\mathbf{L}$, i.e., Eqs. (20)–(22) can largely decrease the complexity in building simulation platform with the four lane traffic model DLM.

Label the l-th ideal weight by $\overline{\varpi}_l, l = 0, 1, 2$, their values are given by Henrick et al. (2005)

$$\overline{\varpi}_0 = 1/10, \quad \overline{\varpi}_1 = 6/10 \text{and} \overline{\varpi}_2 = 3/10. \tag{23}$$

using the indicators of smoothness

$$\left.\begin{array}{l}\beta_0=\frac{13}{12}(\phi_{i-2}-2\phi_{i-1}+\phi_i)^2+\frac{1}{4}(\phi_{i-2}-4\phi_{i-1}+3\phi_i)^2,\\ \beta_1=\frac{13}{12}(\phi_{i-1}-2\phi_i+\phi_{i+1})^2+\frac{1}{4}(\phi_{i+1}-\phi_{i-1})^2,\\ \beta_2=\frac{13}{12}(\phi_{i+2}-2\phi_{i+1}+\phi_i)^2+\frac{1}{4}(\phi_{i+2}-4\phi_{i+1}+3\phi_i)^2.\end{array}\right\}\tag{24}$$

being relevant to variable ϕ, the non-oscillatory weights are (Jiang and Shu, 1996)

$$\omega_l=\frac{\alpha_l}{\sum_{r=0}^{2}\alpha_r},\,\text{where}\alpha_l=\frac{\overline{\omega}_l}{(\epsilon+\beta_l)^2}.\tag{25}$$

where ϵ is a very small number adopted to ensure that the denominator does not vanish and is set to $\epsilon=10^{-40}$ in our numerical tests.

For $\phi=F_k^+, k=1,2,3$, according to Eqs. 24,25, one obtains $\omega_{0,\,k}^+$ and $\omega_{2,\,k}^+$. It is necessary to remind that when $\phi=F_k^-, k=1,2,3$, due to the existence of non-positive eigenvalues, β_0 and β_2 should be mutually alternated, that means we should use

$$\left.\begin{array}{l}\beta_2=\frac{13}{12}(\phi_{i-2}-2\phi_{i-1}+\phi_i)^2+\frac{1}{4}(\phi_{i-2}-4\phi_{i-1}+3\phi_i)^2,\\ \beta_1=\frac{13}{12}(\phi_{i-1}-2\phi_i+\phi_{i+1})^2+\frac{1}{4}(\phi_{i+1}-\phi_{i-1})^2,\\ \beta_0=\frac{13}{12}(\phi_{i+2}-2\phi_{i+1}+\phi_i)^2+\frac{1}{4}(\phi_{i+2}-4\phi_{i+1}+3\phi_i)^2.\end{array}\right\}\tag{26}$$

and Eq. (25) to predict the non-oscillatory weights $\omega_{0,\,k}^-$ and $\omega_{2,\,k}^-$.

Labeling

$$\left.\begin{array}{l}\omega_{0,\,\mathbf{k}}^{\pm}=\mathrm{diag}\left(\omega_{0,\,1}^{\pm},\omega_{0,\,2}^{\pm},\omega_{0,\,3}^{\pm}\right),\\ \omega_{2,\,\mathbf{k}}^{\pm}=\mathrm{diag}\left(\omega_{2,\,1}^{\pm},\omega_{2,\,2}^{\pm},\omega_{2,\,3}^{\pm}\right).\end{array}\right\}\tag{27}$$

and further denoting the time step and spatial node size respectively by Δt and Δx, the WENO5 discretizes $\partial\mathbf{F}(\mathbf{U})/\partial x$ by

$$\frac{\partial\mathbf{F}(\mathbf{U})}{\partial x}|_i=\frac{1}{\Delta x}\left(\widehat{\mathbf{F}}_{i+1/2}-\widehat{\mathbf{F}}_{i-1/2}\right),\tag{28}$$

where numerical flux at mesh face $i+1/2$ is

$$\widehat{\mathbf{F}}_{i+1/2}=\widehat{\mathbf{F}}_{i+1/2}^{+}+\widehat{\mathbf{F}}_{i+1/2}^{-}.$$

Abbreviating $\mathbf{F}^{\pm}(\mathbf{U}_i)$ as $\mathbf{F}_i^{\pm}$, the WENO5 gives the numerical flux as follows Henrick et al. (2005)

$$\left.\begin{array}{rl}\widehat{\mathbf{F}}_{i+1/2}^{+}= & \frac{1}{12}\left(-\mathbf{F}_{i-1}^{+}+7\mathbf{F}_i^{+}+7\mathbf{F}_{i+1}^{+}-\mathbf{F}_{i+2}^{+}\right)+\frac{\omega_{0,\,\mathbf{k}}^{+}}{3}\left(\mathbf{F}_{i-2}^{+}-3\mathbf{F}_{i-1}^{+}+3\mathbf{F}_i^{+}-\mathbf{F}_{i+1}^{+}\right)\\ & +\frac{1}{6}\left(\omega_{2,\,\mathbf{k}}^{+}-0.5\right)\left(\mathbf{F}_{i-1}^{+}-3\mathbf{F}_i^{+}+3\mathbf{F}_{i+1}^{+}-\mathbf{F}_{i+2}^{+}\right),\\ \widehat{\mathbf{F}}_{i+1/2}^{-}= & \frac{1}{12}\left(-\mathbf{F}_{i-1}^{-}+7\mathbf{F}_i^{-}+7\mathbf{F}_{i+1}^{-}-\mathbf{F}_{i+2}^{-}\right)+\frac{\omega_{0,\,\mathbf{k}}^{-}}{3}\left(\mathbf{F}_{i+3}^{-}-3\mathbf{F}_{i+2}^{-}+3\mathbf{F}_{i+1}^{-}-\mathbf{F}_i^{-}\right)\\ & +\frac{1}{6}\left(\omega_{2,\,\mathbf{k}}^{-}-0.5\right)\left(\mathbf{F}_{i+2}^{-}-3\mathbf{F}_{i+1}^{-}+3\mathbf{F}_i^{-}-\mathbf{F}_{i-1}^{-}\right).\end{array}\right\}\tag{29}$$

Note that what WENO5 scheme introduced above is as detailed as possible to implement.

To handle time derivative term, different from source term linearization used previously (Zhang et al., 2018a,b), here we adopt a 3rd order Runge–Kutta scheme which also maintains the TVD property (Shu, 1988; Shu and Osher, 1989). For the convenience of scheme description, defining

$$\mathcal{L}(\mathbf{U})=-\frac{\partial\mathbf{F}(\mathbf{U})}{\partial\mathbf{x}}+\mathbf{S},\tag{30}$$

to seek the numerical solution of

$$\frac{\partial\mathbf{U}}{\partial t}=\mathcal{L}(\mathbf{U}),\tag{31}$$

the 3rd order Runge–Kutta scheme has the form

$$\left\{\begin{array}{l}\mathbf{U}_i^{(1)}=\mathbf{U}_i^n+\Delta t\mathcal{L}(\mathbf{U}^n),\\ \mathbf{U}_i^{(2)}=\left(3\mathbf{U}_i^n+\mathbf{U}_i^{(1)}\right)/4+\Delta t\mathcal{L}\left(\mathbf{U}^{(1)}\right)/4,\\ \mathbf{U}_i^{n+1}=\left(\mathbf{U}_i^n+2\mathbf{U}_i^{(2)}\right)/3+2\Delta t\mathcal{L}\left(\mathbf{U}^{(2)}\right)/3,\end{array}\right.\tag{32}$$

where the superscript n denotes the time level.

Using $\omega = \Delta t/\Delta x$, the Courant–Friedrichs–Lewy (CFL) condition of the numerical method is

$$\begin{aligned} \omega = C_{\mathrm{FL}}/\max|a_{k,i}|, \quad & k = 1,2,3; \\ & i = 0,1,2,\cdots,I_{\max}-1, \end{aligned} \tag{33}$$

where $a_{k,i}$ represents the kth eigenvalue for $\mathbf{A}$ at x_i, $I_{\max}$ is the maximum number of mesh, and the Courant number C_{FL} (Shui, 1998) is fixed at 0.6 to avoid distortion of numerical results.

As shown in Fig. 4, the density dependence of traffic pressure p and sound speed ratio c/c_0 for ρ_0=0.368 [in the unit of jam density ρ_m] is calculated with respect to the road condition. In the numerical tests, depending on whether cars are running in the tunnel or in the normal section, we use the black-dashed and blue-dash-dotted curves labeled by *Tunnel*, or adopt the black-solid and blue-solid curves labeled by *Lane II*. These curves are closely related to the free flow speed v_{fk} and braking distance $X_{\mathrm{br}k}$ [see in Eqs. 10,11], but slightly depend on the density fraction s on lane I.

4. Approaches for travel time

4.1. Based-on grid speed of traffic flow

The numerical tests on the basis of the DLM can output the grid speed of traffic flow, i.e., $u_i(t), i \in [0, I_{\max}]$, i denotes the grid number. In the numerical tests, we have assumed that the spatial grids are uniform, the grid length Δx_k is just the same as the length scale l_0 of traffic flow used in the non-dimensionalization of the DLM equations.

Following the previous work (Zhang et al., 2018a), using a pre-assigned time period Δ_0, the local average speed $\overline{u}_i(t)$ at the grid x_i is

$$\overline{u}_i(t) = \frac{1}{\Delta_0}\int_{t-\Delta_0}^{t} u_i(\xi)d\xi, \tag{34}$$

the grid number i depends on the section index k, as k = 3, the grid is located in the tunnel, otherwise when k = 2 it should be in the normal section. As the road total length is expressed by

$$L = \sum_{\mathrm{k}=2}^{3} L^{(\mathrm{k})}. \tag{35}$$

the instantaneous travel time $T_{\mathrm{t}}(t)$ through the road is

$$T_{\mathrm{t}}(t) = \sum_{\mathrm{k}=2}^{3} T_{\mathrm{t}}^{(\mathrm{k})}(t), \tag{36}$$

where

$$T_{\mathrm{t}}^{(\mathrm{k})}(t) = \sum_i \left[\Delta x_i^{(\mathrm{k})}/\overline{u}_i^{(\mathrm{k})}(t)\right]. \tag{37}$$

$\Delta x_i^{(\mathrm{k})} = l_0$, and Δ_0 is assumed to be 7.5 min. As the propagation and interaction of traffic wave causes evident time dependent properties of traffic speed and density, we have to predict the mean travel time by time averaging of $T_{\mathrm{t}}(t)$, which allows us to calculate the relevant root mean square. The mean travel time T_{tav} and $T_{\mathrm{tav}}^{(\mathrm{k})}$ can be expressed by

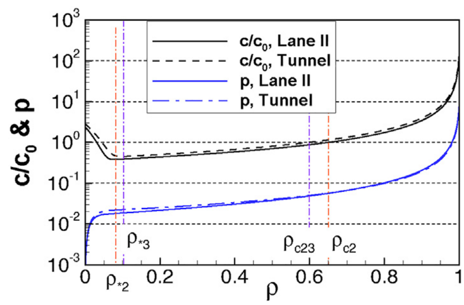

Fig. 4. Sound speed ratio c/c_0 and traffic pressure p versus density ρ. ρ is measured by jam density ρ_m, with p measured by $\rho_m v_{f2}^2$.

$$\begin{cases} T_{\mathrm{tav}} = \frac{1}{t_{\mathrm{end}}-t_{\mathrm{st}}} \int_{t_{\mathrm{st}}}^{t_{\mathrm{end}}} T_{\mathrm{t}}(\xi)d\xi, \\ T_{\mathrm{tav}}^{(\mathrm{k})} = \frac{1}{t_{\mathrm{end}}-t_{\mathrm{st}}} \int_{t_{\mathrm{st}}}^{t_{\mathrm{end}}} T_{\mathrm{t}}^{(\mathrm{k})}(\xi)d\xi. \end{cases} \tag{38}$$

The root mean square T'_{t} and $T_{\mathrm{t}}^{(\mathrm{k})'}$ can be predicted by

$$\begin{cases} \left[T'_{\mathrm{t}}\right]^2 = \frac{1}{t_{\mathrm{end}}-t_{\mathrm{st}}} \int_{t_{\mathrm{st}}}^{t_{\mathrm{end}}} \left[T_{\mathrm{t}}(\xi) - T_{\mathrm{tav}}\right]^2 d\xi, \\ \left[T_{\mathrm{t}}^{(\mathrm{k})'}\right]^2 = \frac{1}{t_{\mathrm{end}}-t_{\mathrm{st}}} \int_{t_{\mathrm{st}}}^{t_{\mathrm{end}}} \left[T_{\mathrm{t}}^{(\mathrm{k})}(\xi) - T_{\mathrm{tav}}^{(\mathrm{k})}\right]^2 d\xi. \end{cases} \tag{39}$$

Where t_{st} is the simulation start time, in general $t_{\mathrm{st}} = 0$, and t_{end} is the simulation end time. Measuring by the time L/v_{f2}, we can define

$$\begin{cases} \sigma_{\mathrm{t}} = T_{\mathrm{t}}/(L/v_{f2}), & \sigma_{\mathrm{tav}} = T_{\mathrm{tav}}/(L/v_{f2}), \quad \sigma'_{\mathrm{t}} = T'_{\mathrm{t}}/(L/v_{f2}), \\ \sigma_{\mathrm{t}}^{(\mathrm{k})} = T_{\mathrm{t}}^{(\mathrm{k})}/(L/v_{f2}), & \sigma_{\mathrm{tav}}^{(\mathrm{k})} = T_{\mathrm{tav}}^{(\mathrm{k})}/(L/v_{f2}), \quad \sigma_{\mathrm{t}}^{(\mathrm{k})'} = T_{\mathrm{t}}^{(\mathrm{k})'}/(L/v_{f2}). \end{cases} \tag{40}$$

4.2. Based-on equilibrium speed

From a technological point of view, the approach based on equilibrium speed at uniform initial density would be the simplest, as it ignores traffic inhomogeneity completely. This approach assumes initial traffic density on the road is uniform, and traffic speed is just equal to the equilibrium speed, which can be determined by the macroscopic fundamental diagram. In the normal segment with length ($L^{(2)}$), the equilibrium speed can be approximated by $(u_{e1} + u_{e2})/2$, while in the freeway tunnel with length $L^{(3)}$, it is u_{e3}. Therefore, the mean travel times through the tunnel and the road can be written as

$$\left.\begin{array}{l} \widehat{\sigma}_{\mathrm{av}}^{(3)} = \frac{L^{(3)}}{u_{e3}} \cdot \frac{v_{f2}}{L}, \\ \widehat{\sigma}_{\mathrm{av}} = \widehat{\sigma}_{\mathrm{av}}^{(3)} + \frac{L^{(2)}}{(u_{e1}+u_{e2})/2} \cdot \frac{v_{f2}}{L}. \end{array}\right\} \tag{41}$$

In practice, the mean travel time should have obvious deviation when this is traffic shock generation and propagation. Hence, for the improvement of σ_{av}, a compensative function $Comp(\rho_0)$ is needed. Suppose the function has a polynomial form

$$Comp(\rho_0) = d_0 + d_1\rho_0 + d_2\rho_0^2 + d_3\rho_0^3, \tag{42}$$

where ρ_0 is initial traffic density normalized by jam density, to estimate mean travel time more accurately, it's better to use

$$\sigma_{\mathrm{av}}^{\star} = \widehat{\sigma}_{\mathrm{av}} + Comp(\rho_0) \tag{43}$$

The polynomial coefficients $d_j, j \in [0, 1, 2, 3]$ can be determined by the case averaged mean travel time obtained on the basis of grid speed of traffic flow.

5. Results and discussion

5.1. Simulation parameters

To predict freeway tunnel effect of travel time, numerical tests of ring traffic flows (Fig. 3) are conducted by the DLM, with the MFD shown in Fig. 1. The 100 km length ring has a tunnel with a length generally assumed to 7.5 km, but the length has been chosen to be 5.0 km, 2.5 km, 1 km, and 0 just for comparison. In the tests, the ratio of characteristic lane changing time to relaxation time represented by $\beta_{\star}$, the three ramp intersections at $X_{\mathrm{R1}}, X_{\mathrm{R2}}, X_{\mathrm{R3}}$, the five initial jams at X_I, ($I = $ A, B, C, D, E), and other traffic flow parameters are shown in Table 1. For instance, it can be seen that $\beta_{\star} = 1$, the traffic length scale l_0 is 100 m, the relevant relaxation times are $\tau_{01}(= l_0/c_{\tau 1} \approx 6.735$ s), $\tau_{02}(= l_0/c_{\tau 2} \approx 9.007$ s), and $\tau_{03}(= l_0/c_{\tau 3} \approx 12.834$ s). The normalized elasticity in the DLM $\widehat{\gamma}$ $\left[= \frac{0.68\times 2G(\tau_0)}{l_0 q_0}\right]$ is 2.178×10^{-3}, relevant to $2\beta = 3.023 \times 10^{-3}$ in the EZM.

The initial density is assumed to be

$$\left.\begin{array}{l} \rho(0,x) = \begin{cases} 1, & \text{for } x =\in [x_I - 1/2, x_I + 1/2], \\ \rho_0, & \text{Otherwise.} \end{cases} \\ \rho_1(0,x) = \begin{cases} 1, & \text{for } x \in [x_I - 1/2, x_I + 1/2], \\ (8/9)\cdot\rho_0, & \text{Otherwise.} \end{cases} \end{array}\right\} \tag{44}$$

with $q(0,x)$=$q_e(\rho(0,x))$. The initial jams are strictly assumed to be positioned at X_I, ($I = $ A, B, C, D, E)[see, in Fig. 2]. These jams' propagation is extremely dependent on the value of ρ_0, the tunnel and ramps, in addition to the traffic sensitivities to the visco-elasticity γ as reported (Smirnova et al., 2017).

5.2. Comparison with EZM

Travel time through the road is an important performance factor of traffic flow evolution. Table 2 listed the mean travel times $\widehat{\sigma}_{\mathrm{av}}$ and $\widehat{\sigma}^{(3)}_{\mathrm{av}}$ that are estimated by Eq. (41)with the approach based-on equilibrium speed at uniform initial density. Obviously, when there exist traffic shocks on the road, the mean travel time is under-predicted, when off-ramp flow plays an overwhelming role of the dynamic traffic than the on-ramp flow, the mean travel time is over-predicted. However, the values in Table 2 provide a sample of reference, and can be further improved by a compensative function $Comp(\rho_0)$ defined by Eq. (42).

Using the same traffic pressure and sound speed expressions, the EZM has been adopted to predict the spatiotemporal density evolution on the ring for the case without ramp effects: $\sigma_{k\mathrm{av}} = 0,\ k \in [1, 2, 3]$. With respect to the grid speed of traffic flow, for the tunnel length $L_{\mathrm{t}} = 7.5\,\mathrm{km}$ the mean travel time through the road σ_{tav}, its root mean square σ'_{t}, the mean travel time through the tunnel $\sigma^{(3)}_{\mathrm{tav}}$, and the corresponding root mean square $\sigma^{(3)\prime}_{\mathrm{t}}$ are predicted, as shown in Table 3. It is seen that for the 13 cases distinguished by ρ_0 in the range from 0.1 to 0.625, the DLM can predict almost certainly the same mean travel times in comparison with the values from the EZM, indicating that the DLM is fairly reliable and reasonable.

The corresponding temporal evolutions of traffic density ρ and acceleration R/ρ are shown in Figs. 5(a-d) for the four cases distinguished by ρ_0. Closely depending on ρ_0, the temporal evolutions of ρ and R/ρ at the ring mid point $x = 50\,\mathrm{km}$ is determined by spatiotemporal evolution of traffic flow. Each peak of density represents the time of a traffic track occurred at the mid point. The recurrent occurrence of traffic track implies the traffic flow has stop–going waves. The curves labeled by EZM and DLM have high similarity, providing the evidence for explaining why the values of mean travel times in Tabel 3 are almost the same.

5.3. Traffic flow patterns

In Figs. 6(a-d), the left and right patterns of traffic flow are corresponding to tunnel length $L_{\mathrm{t}} = X_{\mathrm{t2}} - X_{\mathrm{t1}} = 1$ km and 7.5 km respectively. For $\rho_0 = 0.15$, as shown in Fig. 6(a), the initial traffic jams propagate forward, and so are the jams spontaneously generated between them. These jams are just the traffic tracks used in explaining the temporal evolutions of ρ and R/ρ in Fig. 5(a).

For $\rho_0 = 0.2$, Fig. 6(b) shows that just upstream the tunnel inlet $X_{\mathrm{t1}} = 20\,\mathrm{km}$ cars begin to aggregate and form a traffic shock propagating backward. The shock interacts with the forward spreading jams, causing the congested region being restricted in several kilometers, with the region length depending on the tunnel length to some extent.

For $\rho_0 = 0.368$, as shown in Fig. 6(c), the initial flow is just at the saturation point, the initial jams propagate backward and terminated on the left side of the light blue colored triangle region in the t–x plane, whose bottom is just the tunnel outlet. The tunnel inlet becomes the origin of a congested region spreading backward. Just near the downstream of tunnel outlet, there exists a smooth light blue colored region, in which the density is below 0.2. The smooth region length also depends on the tunnel length to some extent.

For $\rho_0 = 0.5$, initial flow is supersaturated as can be seen in Fig. 6(d), the tunnel effect together with the traffic wave propagation and interaction makes the light blue colored triangle area become smaller. There are some cyan colored oblique lines in the triangle area, these lines represent the traces of spontaneously formed jams or tracks. The light blue color of the triangle area indicates the relevant traffic density is usually below 0.2. As all cars must follow the tunnel speed limit, i.e. 80 km/h, the tunnel has changed the traffic flow patterns and adjusted the propagation and interactions of traffic waves significantly.

Extremely, traffic flow pattern depends on ρ_0. However, Fig. 6 shows that the tunnel length impact on the traffic flow patterns is not quite obvious, to some extent almost negligible.

Table 2
$\widehat{\sigma}_{\mathrm{av}}$, and $\widehat{\sigma}^{(3)}_{\mathrm{av}}$ estimated by Eq. (41) in the case without ramp effects for $L_{\mathrm{t}} = 7.5,\ 5$ and 1 km.

	$L_{\mathrm{t}} = 7.5\,\mathrm{km}$		$L_{\mathrm{t}} = 5\,\mathrm{km}$		$L_{\mathrm{t}} = 1\,\mathrm{km}$	
ρ_0	$\widehat{\sigma}_{\mathrm{av}}$	$\widehat{\sigma}^{(3)}_{\mathrm{av}}$	$\widehat{\sigma}_{\mathrm{av}}$	$\widehat{\sigma}^{(3)}_{\mathrm{av}}$	$\widehat{\sigma}_{\mathrm{av}}$	$\widehat{\sigma}^{(3)}_{\mathrm{av}}$
0.1	1.049	0.094	1.044	0.062	1.035	0.013
0.125	1.161	0.103	1.156	0.069	1.146	0.014
0.15	1.273	0.113	1.267	0.075	1.256	0.015
0.2	1.501	0.133	1.493	0.089	1.481	0.018
0.25	1.742	0.155	1.733	0.103	1.719	0.021
0.3	2.006	0.178	1.996	0.119	1.980	0.024
0.368	2.416	0.215	2.404	0.143	2.384	0.029
0.4	2.636	0.234	2.622	0.156	2.601	0.031
0.45	3.024	0.269	3.009	0.179	2.985	0.036
0.5	3.484	0.309	3.467	0.206	3.439	0.041
0.55	4.040	0.359	4.019	0.239	3.987	0.048
0.6	4.728	0.421	4.705	0.281	4.666	0.056
0.625	5.156	0.474	5.125	0.316	5.074	0.063

Table 3
Density dependence of σ_{tav}, σ'_t, $\sigma^{(3)}_{tav}$, and $\sigma^{(3)\prime}_{tav}$ in the case without ramp effects for $L_t = 7.5$km.

	DLM				EZM			
ρ_0	σ_{tav}	σ'_t	$\sigma^{(3)}_{tav}$	$\sigma^{(3)\prime}_{tav}$	σ_{tav}	σ'_t	$\sigma^{(3)}_{tav}$	$\sigma^{(3)\prime}_{tav}$
0.1	1.0749	0.0021	0.1064	0.0041	1.0748	0.0019	0.1066	0.0036
0.125	1.1817	0.0018	0.1210	0.0054	1.1817	0.0015	0.1211	0.0049
0.15	1.2962	0.0021	0.1387	0.0066	1.2974	0.0024	0.1393	0.0069
0.2	1.5548	0.0099	0.2083	0.0189	1.5547	0.0097	0.2074	0.0188
0.25	1.8794	0.0547	0.2099	0.0148	1.8783	0.0528	0.2124	0.0163
0.3	2.2023	0.0852	0.2118	0.0102	2.2018	0.0843	0.2144	0.0119
0.368	2.6621	0.1087	0.2214	0.0026	2.6579	0.1097	0.2236	0.0018
0.4	2.9344	0.1432	0.2498	0.0044	2.9267	0.1451	0.2406	0.0029
0.45	3.3148	0.1314	0.2768	0.0019	3.3200	0.1317	0.2665	0.0057
0.5	3.7520	0.1467	0.2447	0.0298	3.7476	0.1428	0.2416	0.0308
0.55	4.2544	0.1072	0.2505	0.0376	4.2498	0.1031	0.2472	0.0385
0.6	4.8364	0.0308	0.2560	0.0471	4.8335	0.0286	0.2531	0.0483
0.625	5.2070	0.0188	0.3278	0.0319	5.2070	0.0188	0.3277	0.0319

When ramp effects are further included, for the the cases of $\rho_0 = 0.15, 0.2, 0.368$, and 0.5, the flow patterns are shown in Figs. 7(a-d), where the left and right parts correspond to $\sigma_{2av} = -0.05$, and -0.2 at X_{R2} respectively, with $\sigma_{1av} = 0.1$ and $\sigma_{3av} = -0.1$ fixed at X_{R1} and X_{R3} respectively.

For $\rho_0 = 0.15$, the road is initially unsaturated, see in Fig. 7(a), the on-ramp at $X_{R1} = 17$ km induces the traffic flow in the region near the tunnel inlet $X_{t1} = 20$ km occurs temporary supersaturation, as can be seen in the time period $t \in [0, 5, 1]\,h$. In the right pattern, the traffic ramp discharging at $X_{R2} = 50$ km is larger, when the time is over 0.5 h, the flow downstream the ramp intersection X_{R2} gradually changes to the regime at which the density is below 0.1. While for the off-ramp parameter $\sigma_{2av} = -0.05$, the right pattern is largely different from the right. The ramp input and diversion play a crucial role in the pattern formation of traffic flow.

For $\rho_0 = 0.2$, the road is initially unsaturated, see in Fig. 7(b), and similar to the flow pattern given by Fig. 6(b), a congested region occurs just upstream the tunnel inlet, but the region disappears at the instant of $t \approx 3$ h in the right part of Fig. 7(b), suggesting that ramp discharging is crucial in the flow pattern formation. This can be further confirmed by the spatiotemporal evolutions of traffic density in the cases of $\rho_0 = 0.368$ and 0.5.

For $\rho_0 = 0.368$, the road is initially just at the saturation point, see in Fig. 7(c), the right pattern for $\sigma_{2av} = -0.2$ shows that such a larger ramp discharging can result in a larger smooth region just downstream the off-ramp intersection X_{R2}, in which unless in the spontaneous traffic tracks, the density is below 0.2. In comparison with the left part for $\sigma_{2av} = -0.05$, it is seen that the larger ramp discharging changed the structures of density evolution obviously.

However, when the ring road is initially supersaturated such as for $\rho_0 = 0.5$, as shown in Fig. 7(d), the right pattern indicates that a larger ramp discharging certainly generates the unsaturated region just downstream the off-ramp intersection X_{R2}, similar to the region formed just downstream the tunnel outlet. The right pattern of Fig. 7(d) shows that a further increase of ramp discharging can not only make the traffic flow downstream the ramp intersection from supersaturated to unsaturated regime, but also decrease the traffic density in the near region just upstream the intersection.

The propagation speeds of traffic jams closely depends on the interaction of traffic waves and the MFD used in numerical tests (Daganzo and Daganzo, 1997; Lebacque and Mammar, 2013; Lebacque and Khoshyaran, 2013). As the traffic flow pat-

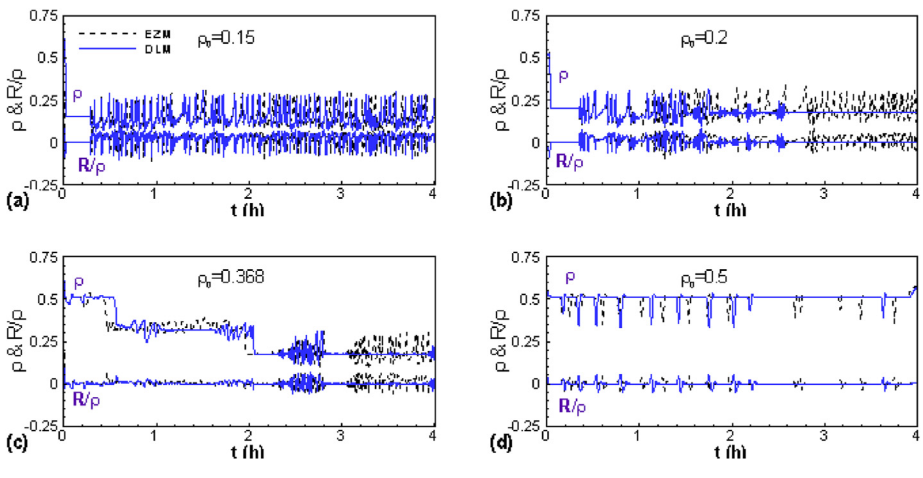

Fig. 5. Temporal evolutions of ρ and R/ρ at $x = 50$ km in the case without ramp effects , (a) $\rho_0 = 0.15$, (b) $\rho_0 = 0.2$, (c) $\rho_0 = 0.368$, (d) $\rho_0 = 0.5$. Note that the legend of part (b), (c) or (d) is the same as shown in part (a) of this figure.

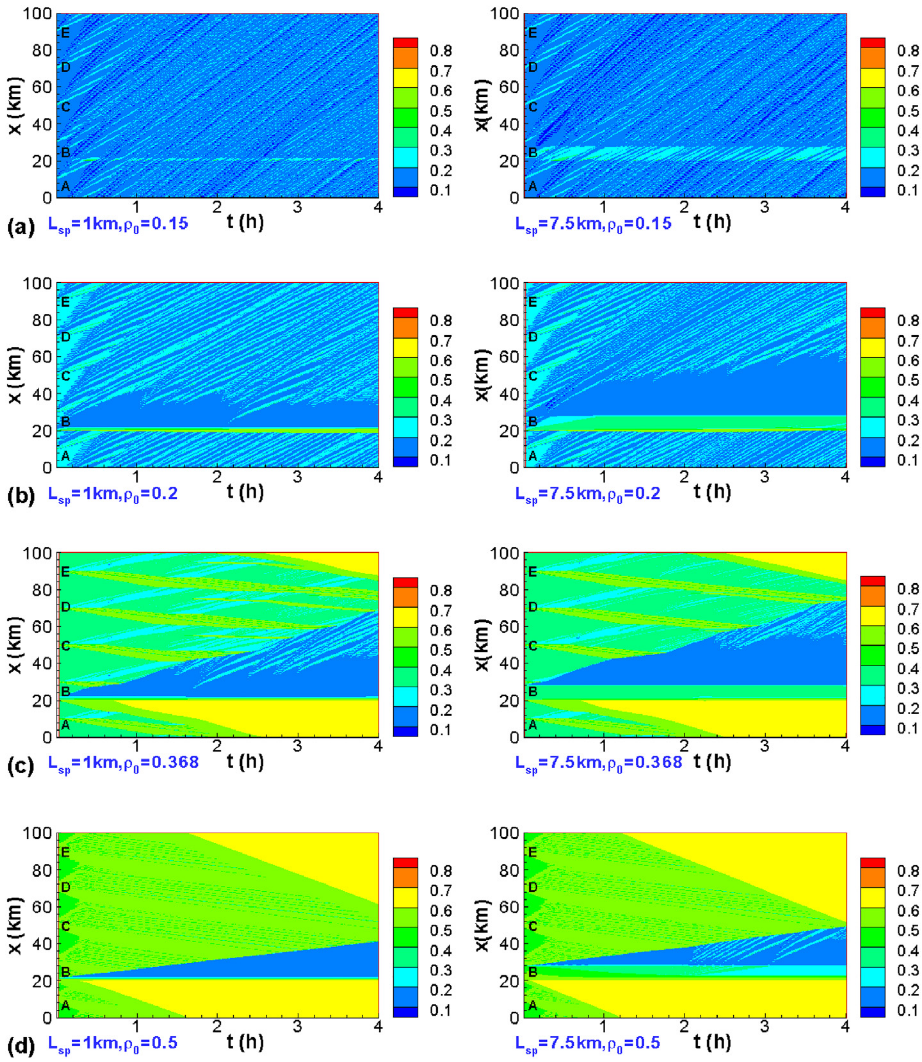

Fig. 6. Spatiotemporal evolutions of traffic density on the ring road for the case without ramp effects , (a)$\rho_0 = 0.15$, (b) $\rho_0 = 0.2$, (c) $\rho_0 = 0.368$, (d) $\rho_0 = 0.5$, with $L_t = 1\,\text{km}$, and $7.5\,\text{km}$ respectively for the left and right patterns.

terns suffer the impacts of road condition significantly, travel time is predicted by the grid speed of traffic flow, suggesting that the road condition effects of travel time should be obvious.

5.4. Instantaneous distributions

For the saturation case, $\rho_0 = \rho_s = 0.368$, being consistent with the flow patterns in Fig. 7(d) and the right part flow pattern in Fig. 7(c), for the tunnel length $L_t = 5\,\text{km}$ and three ramp flow cases labeled by $\sigma_1 = \sigma_2 = \sigma_3 = 0, \sigma_{2av} = -0.05$, and $\sigma_{2av} = -0.2$, the instantaneous distributions of urgent density fraction s on lane I at $t = 0.25, 0.75\,\text{h}$ are shown in Figs. 8(-a-b). From Eq. (1), the equation of s should be

$$\frac{\partial s}{\partial t} + u\frac{\partial s}{\partial x} = (1/2 - s)/(\tau\beta_{\star}) - s\sigma u/l_0$$

the propagation speed of any density fraction disturbance is just the local traffic speed u, but the source term $(1/2 - s)/(\tau\beta_{\star})$ indicates that the expected density fraction is 1/2, with the source term $-s\sigma u$ representing the ramp-flow effects.

In Fig. 8(a), for the case without ramp effects, the black solid line shows the s-distribution at $t = 0.25$ h. In the five initial jams, the initial value of s is set as 0.5, otherwise the initial value of s is given by 4/9, according to Eq. (44). But experiencing the flow evolution of 0.25 h, s-distribution at $t = 0.25\,\text{h}$ becomes a curve around the line given by $s = 1/2$. This is also true for the cases with ramp effects, the s-distribution to some extent depends on the ramp parameter σ_{2av}. Even by further experiencing the flow evolution of 0.25 h, as can be see in Fig. 8(b), the property of the s-distribution maintains, with the absolute maximum deviation to 1/2 below 0.08.

On the other hand, the tunnel and ramp effects on the distributions of traffic density and speed are shown in Figs. 9(a-b) and 10(a-b). In Figs. 9(a-b), the tunnel is labeled by L_t and the maroon dash-dotted square with a width 7.5 km, the density in the tunnel is generally maintain a value approximately identical to $\rho_0 = 0.368$, upstream the tunnel inlet the traffic flow is crowded due to the cars queuing caused by the tunnel speed limit, downstream the tunnel outlet, the traffic flow is smooth and unsaturated, with the smooth length depending on the road operation time. In particular, for the case without ramp effects, the black solid curve shows that the crowded length upstream the tunnel inlet $X_{t1} = 20\,\text{km}$ increases with the operation time period as a results of backward propagation of traffic shock originated at the tunnel inlet. It is seen that the tunnel certainly provides a mechanism of traffic shock generation, and a smooth region just downstream the the tunnel exit $X_{t2} = 27.5\,\text{km}$.

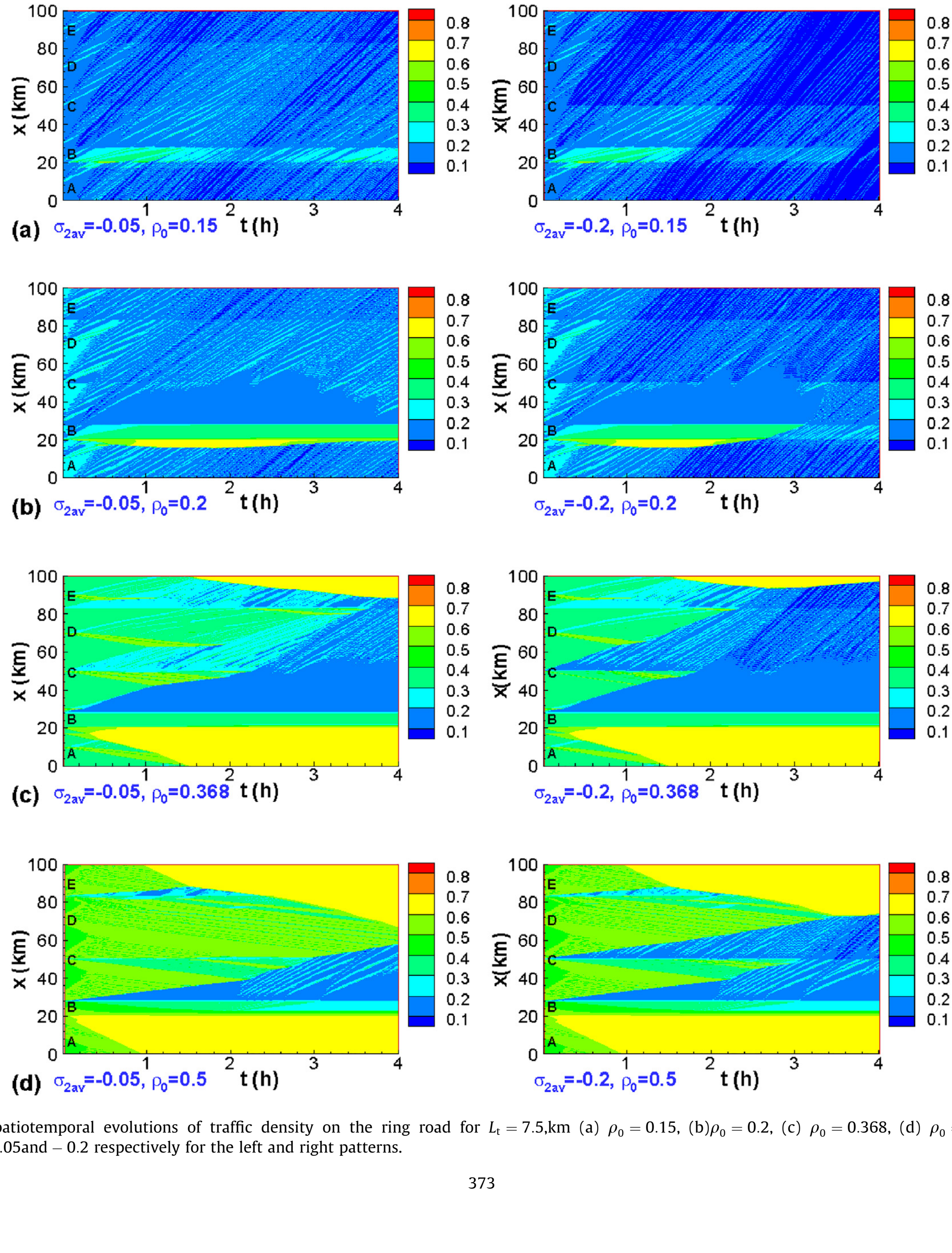

Fig. 7. Spatiotemporal evolutions of traffic density on the ring road for $L_t = 7.5$,km (a) $\rho_0 = 0.15$, (b)$\rho_0 = 0.2$, (c) $\rho_0 = 0.368$, (d) $\rho_0 = 0.5$, with $\sigma_{2av} = -0.05$and $-$ 0.2 respectively for the left and right patterns.

The on-ramp at $X_{R1} = 17\,\text{km}$ increases the degree of road congestion, generate stop–go wave upstream X_{R1} for the case of $\rho_0 = 0.368$, in particular as can be seen from the distributions for the cases of $\sigma_{2av} = -0.05, -0.2$, in the region with several kilometers just upstream the tunnel inlet $X_{t1} = 20\,\text{km}$. Such a special feature of density distribution doesn't occur at the off-ramp intersection $X_{R3} = 83\,\text{km}$, as upstream the off-ramp intersection the density emerges stop-and-going regime, and oscillates around a value 0.6 with a magnitude of about 0.2.

The ramp discharging at $X_{R2} = 60\,\text{km}$ plays a role of providing a smooth region just downstream the intersection. However, for the case of $\sigma_{2av} = -0.2$, the density distributions at the two instants $t = 0.25\,\text{h}$ and $0.75\,\text{h}$ show that upstream the intersection X_{R2} the traffic flow is supersaturated, with a density value around 0.66.

Completely consistent with the density distributions in Figs. 9(a-b), the relevant instantaneous speed distributions for the three cases can be seen in Figs. 10(a-b). A lower density corresponds to a higher speed. The distributions by black solid curves reflect the impact of tunnel on the traffic flow in the case without ramp effects, i.e., σ_{kav}=0, $k = 1,2$ and 3, the green dashed curves and the blue dash-dotted curves reveal the influences from the ramp input and diversion together with tunnel effects on traffic flow on the rind road.

5.5. Comparison with measured data

As shown in Figs. 11(a-d), for the cases of $\sigma_{av2} = -0.05, -0.2$, and tunnel length $L_t = 7.5\,\text{km}$, the the instantaneous speed (u) and equilibrium speed (u_e) at $x = 50\,\text{km}$ are plotted as a function of ρ for $\rho_0 = 0.15, 0.2, 0.368$, and 0.5. The u_e at $x = 50\,\text{km}$ are determined by $u_e = q_e/\rho$, with q_e calculated by Eqs. (5), where some observation data extracted from McShane and Roess (1998) are labeled by symbol '+'.

For $\rho_0 = 0.15$, as can be seen in Fig. 11(a), the left part shows that most traffic state points are scattered in the density range from 0.07 to 0.27, with the right part indicating that most points are scattered in the density range from 0.06 to 0.20. This is consistent with the left and right traffic flow patterns given by Fig. 7(a).

As shown in Fig. 11(b), when $\rho_0 = 0.2$, the left part depicts most traffic state points are scattered in the density range from 0.07 to 0.30, while the right part indicates that most points are scattered in the density range from 0.06 to 0.24, being consistent with the flow patterns in Fig. 7(b).

In Fig. 11(c), it is seen that for $\rho_0 = 0.368$, the ramp discharging $\sigma_{2av} = -0.05$ has induced much flow points located in unsaturated region ($\rho < 0.368$). But the larger ramp discharging $\sigma_{2av} = -0.2$ has caused much more unsaturated traffic flow points. Such observation is also valid for $\rho_0 = 0.5$ as shown in Fig. 11(d). The corresponding evidences can be viewed in Fig. 7(c-d).

Fig. 11 shows that the predicted density dependence of traffic speed usually agrees well with the measured data. Furthermore, re-assigning the tunnel length as $L_t = 1.5\,\text{km}$ instead of $7.5\,\text{km}$, and the time-averaged speed u_{av} and its rms u' for $\rho_0 = 0.368$ near the tunnel in the case without ramp effects are predicted and shown in the left and right parts of Fig. 12. In part (a) of Fig. 12, the observed speed data (Koshi et al., 1992) and the calculated speed on the basis of a behavioral kinematic wave model developed by Jin (2018) are illustrated just for comparison. The predicted speeds agree with the published data rather well, indicating that the DLM is fairly reliable.

5.6. Travel time

Being different from the study of Chang and Mahmassani (1988), in which two heuristic rules are examined, the rules are proposed for describing urban commuters' predictions of travel time as well as the adjustments of departure time in response to unacceptable arrivals in their daily commute under limited information, here we discuss the tunnel effect of the travel time through the ring predicted on the basis of equilibrium speed and grid speed of traffic flow obtained numerically.

As discussed in subSection 5.2, the mean travel times estimated on the basis of equilibrium speed can be found in Table 2. These times have a value of reference, but needs to be further improved by a compensative function $Comp(\rho_0)$ for more accu-

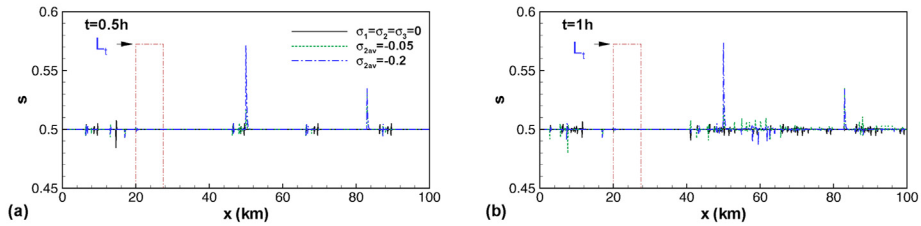

Fig. 8. Distribution of urgent density fraction s for $\rho_0 = 0.368$ at (a) $t = 0.5\,\text{h}$, (b) $t = 1\,\text{h}$. Note that the legend of part (b) is the same as shown in part (a) of this figure.

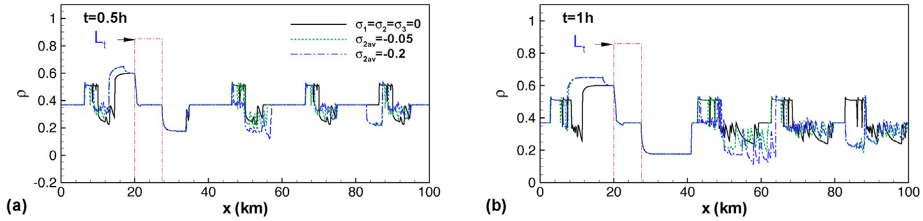

Fig. 9. Distribution of traffic density ρ for $\rho_0 = 0.368$ at (a) $t = 0.5\,\text{h}$, (b) $t = 1\,\text{h}$. Note that the legend of part (b) is the same as shown in part (a) of this figure.

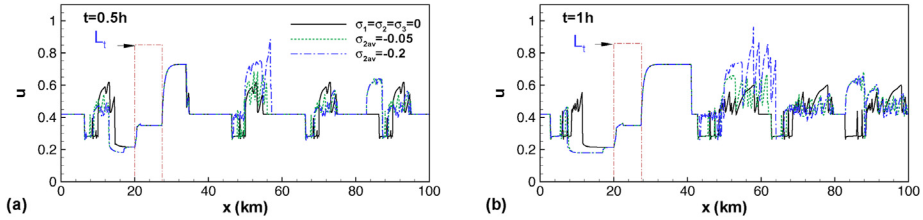

Fig. 10. Distribution of traffic speed u for $\rho_0 = 0.368$ at (a) $t = 0.5\,\text{h}$, (b) $t = 1\,\text{h}$. Note that the legend of part (b) is the same as shown in part (a) of this figure.

rate prediction. Hence, we show the travel time predicted by using grid speed at first and then discuss how to build $Comp(\rho_0)$.

Affected merely by the tunnel in the case without ramp effects, as a response to almost the same flow patterns given by Figs. 6(a-d), the mean travel time σ_{tav} should be almost completely identical to the values predicted for $L_t = 7.5\,\text{km}$ as shown in Table 3, and the mean travel time and its rms for $L_t = 5\,\text{km}$ and 1 km are shown in Table 4. As shown in Figs. 13(a-d), the predicted $\sigma_{\text{tav}}, \sigma_t\prime, \sigma_{\text{tav}}^{(3)}, \sigma_t^{(3)\prime}$, for $L_t = 5\,\text{km}$ and 1 km are almost the same as the values for $L_t = 7.5\,\text{km}$, suggesting that the tunnel length effect of travel time is almost negligible. The tunnel plays a role of enlarging the travel time in comparison with the black line with purple color filled circles for the case of zero tunnel length, this role becomes more evident for the cases of initial density near the saturation point, i.e., $\rho_0 \sim \rho_s$. According to the numerically predicted σ_{tav}, to get the fitted travel time σ_{tf} by linear regression analysis after logarithm processing (Wang et al., 1979), for the case without ramp effects we have

$$\sigma_{\text{tf}} = A\rho_0^m + b \tag{45}$$

where $A = 8.5305, m = 1.5418, b = 0.8230, \rho_0$ has the unit of ρ_m. In the regression analysis, b is calculated with the test-repeating number ($= 6$) averaged values of σ_{tav} at the three points: $\rho_{01} = 0.1, \rho_{02} = 0.25$, and $\rho_{03} = 0.625$, since the root of the product $(\rho_{01} \cdot \rho_{03})$ is just equal to ρ_{02}. The linear regression after logarithm processing has a linear correlation coefficient of 0.9998, with a residual standard deviation of 0.91%. Here the so-called test refers to the numerical tests with various initial densities from 0.1 to 0.625, as given by Table 3. In Fig. 13(a), the fitted expression is illustrated by the light green solid curve.

Fig. 13(b) shows that the root mean square of travel time σ_t' is in general below 0.17, but can be as low as 0.01 for $\rho_0 \leqslant 0.15$. As can be seen in Fig. 13(c), for $L_t \leqslant 2.5\,\text{km}$, if ρ_0 is over 0.2, the mean time through the tunnel $\sigma_{\text{tav}}^{(3)}$ is to a large extent insensitive to the variation of ρ_0, otherwise it grows almost linearly with the increase of ρ_0. Being consistent with the root mean square values given in Tables 2,3, Fig. 13(d) indicates that $\sigma_t^{(3)\prime}$ is usually below 0.055.

The ramp effects can be seen more clearly in Figs. 14(a-d), where the initial density dependencies on $\sigma_{\text{tav}}, \sigma_t', \sigma_{\text{tav}}^{(3)}$, and $\sigma_{\text{tav}}^{(3)\prime}$ for $L_t = 7.5\,\text{km}$ are illustrated. The ramp discharging shortens the mean travel time σ_{tav} [Fig. 14(a)], adjusts the root mean square value σ_t' [Fig. 14(b)]. However, the ramp discharging has less effects on the mean travel time through the tunnel [Fig. 14(c)], and so is $\sigma_{\text{tav}}^{(3)\prime}$ [Fig. 14(d)], since the tunnel inlet has become the origin of a traffic congestion region propagating backward when the initial density is over 0.2 as illustrated in Figs. 7(c-d).

Using $\sigma_{2\text{av}}$ to distinguish the numerical test for the prediction of σ_{tav}, the test repeating number ($= 4$) averaged values of σ_{tav} can be obtained for a given density ρ_0 , these averaged values of σ_{tav} have been used in the regression analysis after logarithm processing (Wang et al., 1979), for the case with ramp effect we have

$$\sigma_{\text{tf}} = A^*\rho_0^{m^*} + b^* \tag{46}$$

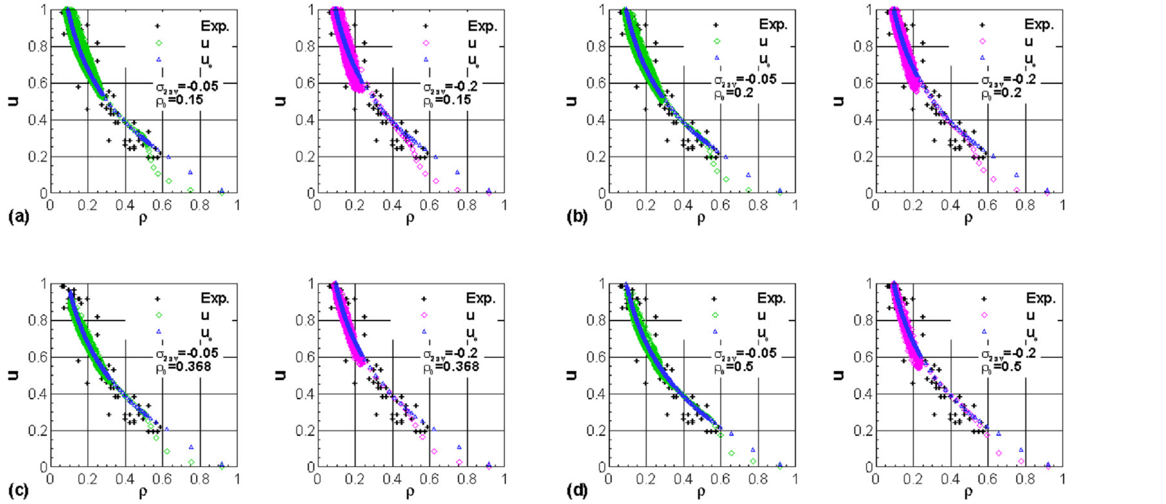

Fig. 11. Comparison of traffic speed with existing measured data for $L_t = 7.5\,\text{km}$ with ramp effect, (a) $\rho_0 = 0.15$; (b) $\rho_0 = 0.2$; (c) $\rho_0 = 0.368$; (d) $\rho_0 = 0.5$. The observation data used in parts (a-d) are obtained from McShane and Roess (1998), and the jam density for normalization is assumed to be 200 veh/mile.

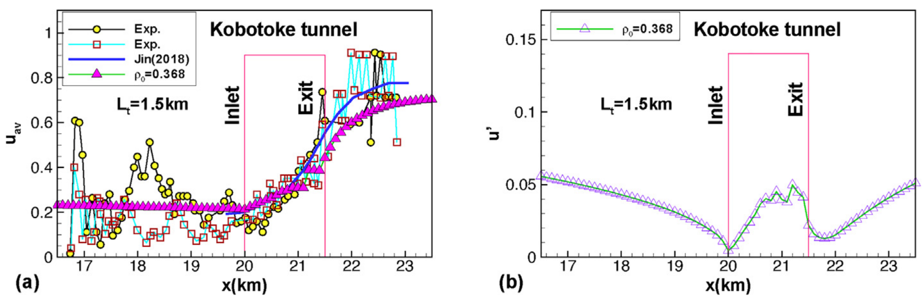

Fig. 12. Comparison of time-averaged speed u_{av} for $\rho_0 = 0.368$ with that some existing data as shown in the left part of this figure, with the relevant curves for the rms value u' given in right part. The two speed trajectories with legend 'Exp.' are recorded at the Kobotoke tunnel in Japan (Koshi et al., 1992), the calculated speed labeled by the blue solid curve are abstracted from Jin (2018). Note that the abstracted data are normalized by v_{f2}.

Table 4
Density dependence of σ_{tav}, σ'_t, $\sigma^{(3)}_{tav}$, and $\sigma^{(3)\prime}_{tav}$ in the case without ramp effects for $L_t = 5$ and 1 km.

	$L_t = 5\,\text{km}$				$L_t = 1\,\text{km}$			
ρ_0	σ_{tav}	σ'_t	$\sigma^{(3)}_{tav}$	$\sigma^{(3)\prime}_{tav}$	σ_{tav}	σ'_t	$\sigma^{(3)}_{tav}$	$\sigma^{(3)\prime}_{tav}$
0.1	1.0685	0.0020	0.0708	0.0038	1.0586	0.0016	0.0130	0.0012
0.125	1.1736	0.0015	0.0809	0.0045	1.1629	0.0011	0.0150	0.0013
0.15	1.2891	0.0021	0.0935	0.0054	1.2761	0.0016	0.0178	0.0022
0.2	1.5452	0.0091	0.1451	0.0119	1.5259	0.0080	0.0371	0.0032
0.25	1.8694	0.0552	0.1462	0.0096	1.8489	0.0536	0.0382	0.0026
0.3	2.1930	0.0857	0.1470	0.0072	2.1719	0.0815	0.0383	0.0024
0.368	2.6511	0.1067	0.1501	0.0022	2.6316	0.1019	0.0384	0.0020
0.4	2.9256	0.1453	0.1821	0.0085	2.8609	0.1137	0.0397	0.0021
0.45	3.3058	0.1372	0.1880	0.0038	3.2317	0.0990	0.0414	0.0006
0.5	3.7359	0.1495	0.1698	0.0139	3.6458	0.1117	0.0415	0.0002
0.55	4.2290	0.1078	0.1726	0.0185	4.1273	0.0700	0.0416	0.0002
0.6	4.7975	0.0320	0.1747	0.0235	4.6914	0.0002	0.0423	0.0008
0.625	5.1615	0.0090	0.2165	0.0163	5.0978	0.0004	0.0471	0.0007

where $A^* = 8.5321, m^* = 1.5248, b^* = 0.7789$, ρ_0 is in the unit of ρ_m. Note that the regression of $\log_{10}A^*$ and m^* has a linear correlation coefficient of 0.9999, with a residual standard deviation of about 0.74%. The expression is shown by the light green solid curve in Fig. 14(a).

In the case without ramp effects, to build the compensative function $Comp(\rho_0)$ in the form of Eq. 42, we at first calculate the deviation of mean travel time $\delta\sigma_{tav}\,(= \sigma_{tav} - \sigma_{av})$ for the four cases: $L_t = 7.5$, 5, 2.5 and 1 km, excluding the case of $L_t = 0$;

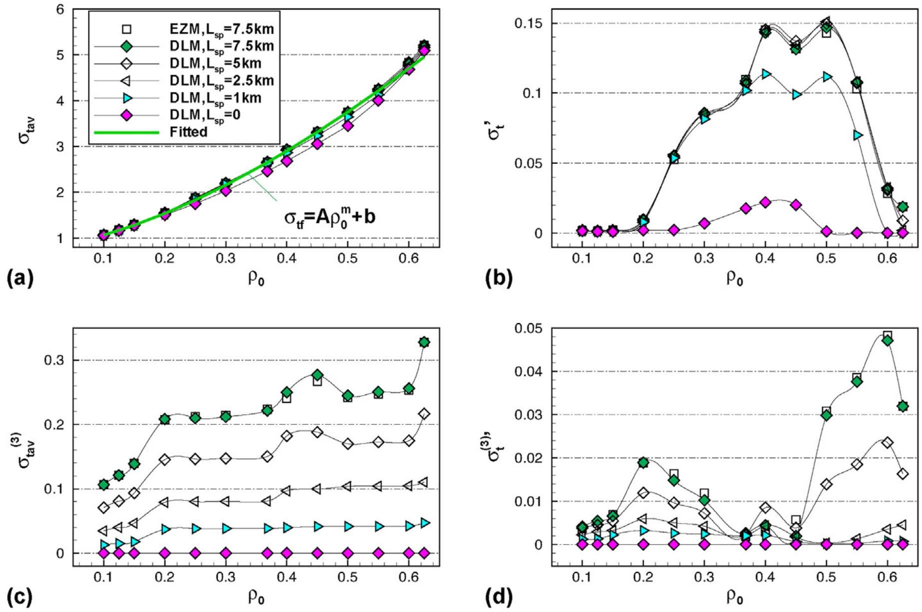

Fig. 13. Density dependence of (a) σ_{tav}, (b) σ_{t}', (c) $\sigma_{\text{tav}}^{(3)}$, and (d) $\sigma_{\text{t}}^{(3)\prime}$ at different tunnel lengths for the case without ramp effects: $\sigma_{1\text{av}}$=$\sigma_{2\text{av}}$=$\sigma_{3\text{av}}$=0. Note that for the fitted curve in part (a): $A = 8.5305, m = 1.5418, b = 0.8230$; the legend of part (b), (c) or (d) is the same as shown in part (a) of this figure.

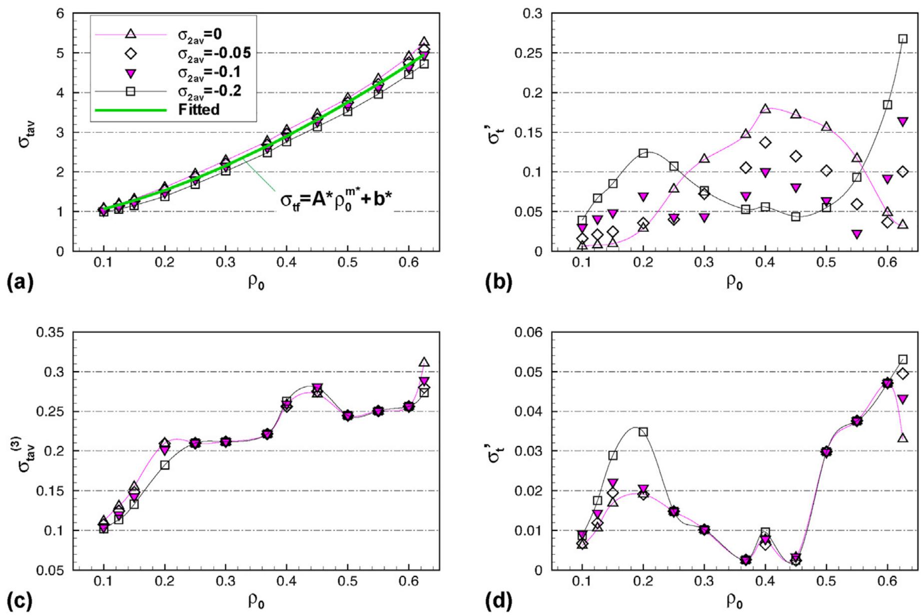

Fig. 14. Density dependence of (a) σ_{tav}, (b) σ_{t}', (c) $\sigma_{\text{tav}}^{(3)}$, and (d) $\sigma_{\text{t}}^{(3)\prime}$ for tunnel length $L_{\text{t}} = 7.5$ km in the case with ramp effect. Note that for the fitted curve in part (a): $A^* = 8.5321, m^* = 1.5248, b^* = 0.7789$; the legend of part (b), (c) or (d) is the same as shown in part (a) of this figure.

then calculate the case averaged values of the deviation $\delta\sigma_{\text{tav}}$, fitting the case averaged data of the deviation, one obtains the polynomial coefficients $d_j, j \in [0, 1, 2, 3]$, as given by in Table 5. The fitted curve represents the compensative function, as can be seen in Fig. 15(a). On the other hand, in the case with ramp effects, the deviation of mean travel time $\delta\sigma_{\text{tav}}$ corresponds to the four cases distinguished by $\sigma_{2\text{av}} = 0, -0.05, -0.1$, and -0.2. The polynomial coefficients for $Comp(\rho_0)$ are also listed in Table 5, with the fitted curve shown in in Fig. 15(b).

Generally say, after using $Comp(\rho_0)$, the deviation of mean travel time predicted by using equilibrium speed is less than 5 min, in comparison with the mean travel time predicted numerically on the basis of grid speed of traffic flow.

Table 5
Fitted coefficients of $Comp(\rho_0)$ for $\rho_0 \in [0.1, 0.625]$.

d_0	d_1	d_2	d_3
	Without ramp effects		
0.06468	−1.3675	9.4175	−11.7735
	With ramp effects		
0.13200	−2.9177	15.4555	−18.4597

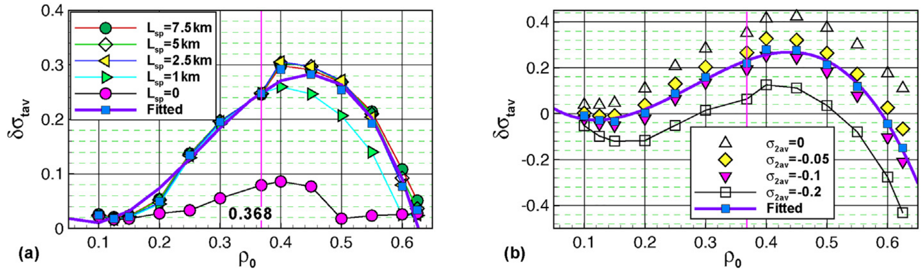

Fig. 15. $\delta\sigma_{\text{tav}}$ plotted as a function of ρ_0, (a) without ramp effects, (b) with ramp effects. Note that $\delta\sigma_{\text{tav}} = \sigma_{\text{tav}} - \sigma_{\text{av}}$, the fitted coefficients for compensative function $Comp(\rho_0)$ are given in Table 5.

6. Conclusions

To explore freeway tunnel effect of travel time, a double lane traffic model (DLM) is developed, a compensative function of mean travel time is simply introduced, and a simulation platform is built to predict the spatiotemporal evolution of traffic flow. The freeway tunnel is assumed to have a length of 7.5 km except for the case of seeking the tunnel length effects. The mean travel time can be predicted either numerically or by another approach based on equilibrium speed at uniform initial density with the compensative function. From the results discussed in the foregoing section, we can list the conclusions as below:

1. The DLM provides a simple approach to describe the net lane-changing rate on freeways. It can be used to simulate double lane traffic flows, predict the travel time.
2. The freeway tunnel impacts the traffic flow pattern significantly. When the road initial density measured by jam density is over 0.2, there exists a congestion region just upstream the tunnel inlet. While a smooth section occurs just downstream the tunnel exit where the traffic flow is unsaturated.
3. The on/off ramp flows are also crucial in the formation of traffic flow pattern. There is also a smooth section just downstream the off-ramp intersection, the larger the ramp discharging, the longer the smooth section.
4. The urgent density fraction has an expected value of 1/2, for instance, its distribution at the time of 0.5 h indicates that the absolute value of maximum deviation to 1/2 is below 0.08.
5. The tunnel can increase the mean travel time through the road in some extent, but its length effect on the mean travel time is small and almost negligible. Using the regression analysis after logarithm processing, the fitted expression can be obtained.
6. The approach for mean travel time based-on equilibrium speed at uniform initial density with a compensative function would be the simplest from a technological point of view, it can estimate the mean travel time with a deviation generally less than 5 min, in comparison with the mean travel time predicted numerically.

Declaration of Competing Interest

The authors declare that they have no known competing financial interests or personal relationships that could have appeared to influence the work reported in this paper.

Acknowledgements

This work is supported by National Natural Science Foundation of China (Grant 11972341), Russian Foundation for Basic Research (Grant 18–07-00518) and fundamental research project of Lomonosov Moscow State University ‘Mathematical models for multi-phase media and wave processes in natural, technical and social systems’. We thank Dr. Y.L. Li at Peking University for some useful private communications.

References

Aw, A., Rascle, M., 2000. Resurrection of second order models of traffic flow. SIAM J. Appl. Math. 60, 916–938.

Borges, R., Carmona, M., Costa, B., Don, W.S., 2008. An improved weighted essentially non-oscillatory scheme for hyperbolic conservation laws. J. Comput. Phys. 227, 3191–3211.

Chang, G.L., Mahmassani, H.S., 1988. Travel time prediction and departure time adjustment behavior dynamics in a congested traffic system. Transp. Res. Part B: Methodol. 22 (2), 217–232.

Chang, G.L., Zhu, Z.J., 2006. A macroscopic traffic model for highway work zones: formulations and numerical results. J. Advanced Transp. 40 (3), 265–287.

Daganzo, C.F., 1995. Requiem for second-order fluid approximations of traffic flow. Transp. Res. Part B: Methodol. 29, 277–286.

Daganzo, C.F., 1997. Traffic flow theory. In: Daganzo, C.F. (Ed.), Fundamentals of Transportation and Traffic Operations. Pergamon, New York, pp. 67–160.

Daganzo, C.F., 2002. A behavioral theory of multi-lane traffic flow. part i: Long homogeneous freeway sections. Transp. Res. Part B: Methodol. 36, 131–158.

Daganzo, C.F., 2002. A behavioral theory of multi-lane traffic flow: Part ii: Merges and onset of congestion. Transp. Res. Part B: Methodol. 36, 159–169.

Davis, L.C., 2004. Multilane simulations of traffic phases. Phys. Rev. E 69, 016108.

Papageorgiou, M. 2014. High-resolution numerical relaxation approximations to second-order macroscopic traffic flow models. Transp. Res. Part C: Emerg. Technol. 44, 318–349.

Günther, G., Coeymans, J.E., Muñoz, J.C., Herrera, J.C. 2012. Mitigating freeway off-ramp congestion: A surface streets coordinated approach. Transp. Res. Part C: Emerging Technologies 20, 112–125.

Haight, F.A., 1963. Mathematical theories of traffic flow. Academic Press, New York.

Helbing, D., Treiber, M., 1998. Gas-kinetic-based traffic model explaining observed hysteretic phase transition. Phys. Rev. Lett. 81, 3042–3045.

Henrick, A.K., Aslam, T.D., Powers, J.M., 2005. Mapped weighted essentially non-oscillatory schemes: Achieving optimal order near critical points. J. Comput. Phys. 207, 542–567.

Hoogendoorn, S.P., Bovy, P.H.L., 2000. Continuum modeling of multiclass traffic flow. Transp. Res. Part B: Methodol. 34 (2), 123–146.

Jiang, G.S., Shu, C.W., 1996. Efficient implementation of weighted eno schemes. J. Comput. Phys. 126, 202–228.

Jin, W.L., 2010. A kinematic wave theory of lane-changing traffic flow. Transp. Res. Part B: Methodol. 44 (8–9), 1001–1021.

Jin, W.L., 2013. A multi-commodity lighthillwhithamrichards model of lane-changing traffic flow. Transp. Res. Part B: Methodol. 57, 361–377.

Jin, W.L., 2018. Kinematic wave models of sag and tunnel bottlenecks. Transp. Res. Part B: Methodol. 107, 41–56.

Kerner, B., Konhäuser, P., 1993. Cluster effect in initially homogemeous traffic flow. Phys. Rev. E 48, 2335–2338.

Kiselev, A.B., Nikitin, V.F., Smirnov, N.N., Yumashev, M.V. 2000. Irregular traffic flow on a ring road. J. Appl. Math. & Mech. 64(4), 627–634.

Koshi, M, Kuwahara, M, Akahane, H. 1992. Capacity of sags and tunnels on japanese motorways. ITE J. 62(5), 17–22.

Laval, J.A., Daganzo, C.F., 2006. Lane-changing in traffic streams. Transp. Res. Part B: Methodol. 40, 251–264.

Lebacque, J.P., Khoshyaran, M.M., 2013. A variational formulation for higher order macroscopic traffic flow models of the gsom family. Transp. Res. Part B: Methodol. 57, 245–265.

Lebacque, J.P. and Haj-Salem, H. 2007. Generic second order traffic flow modelling, in: Allsop, R., Benjiamin, G. (Eds.), Transportation and Traffic Theory. Elsevier: Oxford, pp. 755–776.

Li, L., Chen, X.Q., 2017. Vehicle headway modeling and its inferences in macroscopic/ microscopic traffic flow theory: A survey. Transp. Res. Part C: Emerging Technologies 76, 170–188.

Li, P.F., Souleyrette, R.R., 2016. A generic approach to estimate freeway traffic time. Comput.-Aid. Civ. Infrastr. Eng. 31, 351–365.

Lighthill, M.J., Whitham, G.B., 1955. On kinematic waves ii: a theory of traffic flow on long crowded roads. Proc. Roy. Soc. Lond A 229, 317–345.

Liu, H., Kan, X.G., Shladover, S.E., Lu, X.Y., Ferlis, R.E., 2018. Modeling impacts of cooperative adaptive cruise control on mixed traffic flow in multi-lane freeway facilities. Transp. Res. Part C: Emerg. Technol. 95, 261–279.

Ma, J., Chan, C.K., Ye, Z.B., Zhu, Z.J. 2018. Effects of maximum relaxation in viscoelastic traffic flow modeling. Transp. Res. Part B: Methodol. 113, 143–163.

McShane, W.R., Roess, R.P., Prassas, E.S. 1998. Calibration relationships for freeway analysis, in: McShane, W.R., Roess, R.P., Prassas, E.S. (Eds.), Traffic Engineering. Prentice-Hall: New Jersey, pp. 282–306.

Michalopoulos, P.G., Beskos, D.E., Lin, J. 1984. Analysis of interrupted traffic flow by finite difference methods. Transp. Res. Part B: Methodol. 18(4–5), 409–421.

Nagatani, T., 2002. The physics of traffic jams. Rep. Prog. Phys. 65, 1331–1386.

Payne, H.J. 1971. Models of freeway traffic and control. In: Mathematical Model of Public Systems, Simulation Council Proc. La Jola California 1, 51–61.

Rascle, M., 2002. An improved macroscopic model of traffic flow: derivation and links with the lighthill-whitham model. Math. Comput. Model. 35, 581–590.

Richards, P.I., 1956. Shock waves on the freeway. Operations Res. 4, 42–51.

Shu, C.W., 1988. Total-variation-diminishing time discretizations. SIAM J. on Scientific and Statistical. Computing 9, 1073–1084.

Shu, C.W., Osher, S., 1989. Efficient implementation of essentially non-oscillatory shock-capturing schemes. J. Comput. Phys. 83, 32–78.

Shui, H.S. 1998. TVD scheme, in: Shui, H.S. (Ed.), Finite Difference in One-dimensional Fluid Mechanics. National Defense: Beijing, in Chinese, pp. 333–355.

Smirnova, M.N., Bogdanova, A.I., Zhu, Z.J., Smirnov, N.N. 2017. Traffic flow sensitivity to parameters in viscoelastic modelling. Transportmetrica B: Transport Dynamics 5(1), 115–131.

Tang, T.Q., Wang, Y.P., Yang, X.B., Huang, H.J., 2014. A multilane traffic flow model accounting for lane width, lane-changing and the number of lanes. Networks Spatial Econom. 14, 465–483.

Tang, T.Q., Wong, S.C., Huang, H.J., Zhang, P., 2008. Macroscopic modeling of lane-changing for two-lane traffic flow. J. Adv.Transp. 43 (3), 245–273.

Tao, W.Q. 2001. Numerical heat transfer, Xian Jiantong University Press: Xi'an (in Chinese), pp. 195–251.

Wang, L.X., Fang, D.Z., et al. 1979. Regression analysis, in: Wang, Y., Wan, Z.X. (Eds.), Handbook of Mathematics. Higher Education Press: Beijing, in Chinese, pp. 836–847.

Wang, P.C., Yu, G.Z., Wu, X.K., Wang, Y.P., He, X.Z. 2019. Spreading patterns of malicious information on single-lane platooned traffic in a connected. Computer-Aided Civil and Infrastructure Engineering 34, 248–265.

Xie, Z.M., Zhu Z.J., Hu, J.J. 2006. Numerical study of mixed freeway traffic flows. Communications in Numerical Methods in Engineering 22(1), 33–39.

Xu, R.Y., Zhang, P., Dai, S.C., Wong, S.C. 2007. Admissibility of a wide cluster solution inanisotropic higher-order traffic flow models. SIAM J. Appl. Math. 68 (2), 562–573.

Zhang, H.M., 2003. Driver memory, traffic viscosity and a viscous vehicular traffic flow model. Transp. Res. Part B: Methodol. 37, 27–41.

Zhang, W.H., Yan, R., Feng, Z.X., Wang, K., 2016. Study of highway lane-changing model under rain weather. Acta Phys. Sin. 65, (6) 064501.

Zhang, H., Ritchie, S.G., Recker, W.W. 1996. Some general results on the optimal ramp control problem. Transp. Res. Part C: Emerging Technologies 4(2), 51–69.

Zhang, P., Wong, S.C., Dai, S.Q. 2009. A conserved higher order aniso-tropic traffic flow model: Description of equilibrium and non-equilibrium flows. Transp. Res. Part B: Methodol. 43(5), 562–574.

Zhang, Y.L., Smirnova, M.N., Bogdanova, A.I., Zhu, Z.J., Smirnov, N.N. 2018a. Travel time estimation by urgent-gentle class traffic flow model. Transp. Res. Part B: Methodol. 113, 121–142.

Zhang, Y.L., Smirnova, M.N., Bogdanova, A.I., Zhu, Z.J., Smirnov, N.N. 2018b. Travel time prediction with a viscoelastic traffic model. Applied Math. & Mech. (English Edition) 39(12), 1769–1788.

Zheng, Z.D., 2014. Recent developments and research needs in modeling lane changing. Transp. Res. Part B: Methodol. 60, 16–32.

Zheng, L., He, Z.B., He, T. 2017. An anisotropic continuum model and its calibration with an improved monkey algorithm. Transportmetrica A: Transport Science 13(6).

Zhu, Z.J., Wu, T.Q., 2003. Two-phase fluids model for freeway traffic and its application to simulate the evolution of solitons in traffic. ASCE. J. Transp. Eng. 129, 51–56.
Zhu, Z.J., Yang, C., 2013. Visco-elastic traffic flow model. J. Adv. Transp. 47, 635–649.
Zhu, Z.J., Chang, G.L., Wu, T.Q., 2004. Numerical analysis of freeway traffic flow dynamics under multiclass drivers. Transp. Res. Rec. 1852, 201–219.